═══REVIEW COMMONS MANUSCRIPT═══

IMPORTANT:

- Manuscripts submitted to Review Commons are peer reviewed in a journal-agnostic way.
- Upon transfer of the peer reviewed preprint to a journal, the referee reports will be available in full to the handling editor.
- The identity of the referees will NOT be communicated to the authors unless the reviewers choose to sign their report.
- The identity of the referee will be confidentially disclosed to any affiliate journals to which the manuscript is transferred.

GUIDELINES:

- For reviewers: https://www.reviewcommons.org/reviewers
- For authors: https://www.reviewcommons.org/authors

CONTACT:

The Review Commons office can be contacted directly at: office@reviewcommons.org

TopBP1 biomolecular condensates: a new therapeutic target in advanced-stage colorectal cancer.

Laura Morano[1], Nadia Vezzio-Vié[2], Adam Aissanou[2], Tom Egger[1], Antoine Aze[1], Solène Fiachetti[1], Hervé Seitz[1], Louis-Antoine Milazzo[2], Véronique Garambois[2], Nathalie Bonnefoy[2], Céline Gongora[2,3*], Angelos Constantinou[1,4], Jihane Basbous[1,3*]

1. Institut de Génétique Humaine, Univ Montpellier, CNRS, Montpellier, France

2. IRCM, Univ Montpellier, ICM, INSERM, Montpellier, France

3. Lead contact

4. Deceased

* Correspondence: jihane.basbous@igh.cnrs.fr, celine.gongora@inserm.fr

Graphical abstract

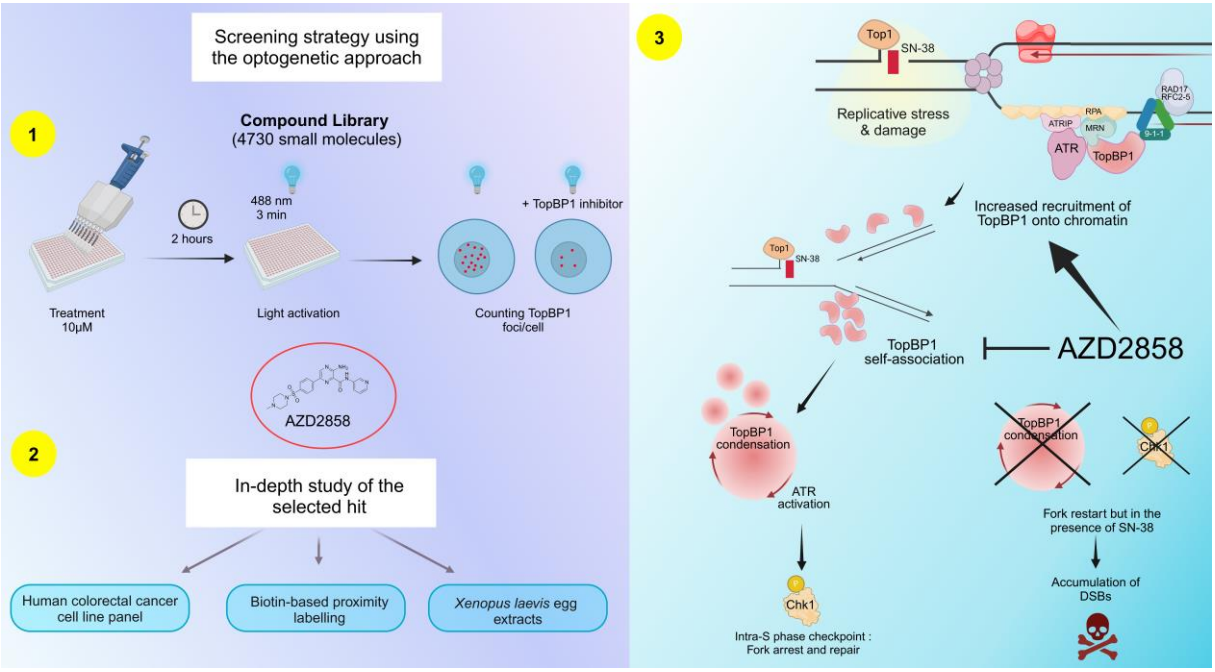

Abstract

In cancer cells, ATR signaling is crucial to tolerate the intrinsically high damage levels that normally block replication fork progression. Assembly of TopBP1, a multifunctional scaffolding protein, into condensates is required to amplify ATR kinase activity to the levels needed to coordinate the DNA damage response and manage DNA replication stress. Many ATR inhibitors are tested for cancer treatment in clinical trials, but their overall effectiveness is often compromised by the emergence of resistance and toxicities. In this proof-of-concept study, we propose to disrupt the ATR pathway by targeting TopBP1 condensation. First, we screened a molecule-based library using a previously developed optogenetic approach and identified several TopBP1 condensation inhibitors. Amongst them, AZD2858 disrupted TopBP1 assembly induced by the clinically relevant topoisomerase I inhibitor SN-38, thereby inhibiting the ATR/Chk1 signaling pathway. We found that AZD2858 exerted its effects by disrupting TopBP1 self-interaction and binding to ATR in mammalian cells, and by increasing its chromatin recruitment in cell-free *Xenopus laevis* egg extracts. Moreover, AZD2858 prevented S-phase checkpoint induction by SN-38, leading to increased DNA damage and apoptosis in a colorectal cancer cell line. Lastly, AZD2858 showed synergistic effect in combination with the FOLFIRI chemotherapy regimen in a spheroid model of colorectal cancer.

Introduction

In every cell, thousands of DNA lesions are induced by endogenous and environmental agents (1). To overcome their deleterious effects, cells have evolved an intricate network of DNA damage response pathways that detect, signal and repair DNA lesions. These pathways work in coordination with key physiological processes, such as cell cycle progression, chromatin remodeling, and transcription (2,3). Cancer cells typically exhibit higher levels of genotoxic stress than non-transformed cells due to their altered metabolism and high proliferation rate (4–6). As a complement to radiotherapy and chemotherapy that overload cancer cells with DNA lesions, the aim of novel anti-cancer strategies is to increase the sensitivity of cancer cells to genotoxic stress by targeting DNA damage signaling and DNA repair mechanisms (4,7).

For example, ATR signaling activates cell cycle checkpoints (8–10), promotes DNA repair (11), regulates the firing of replication origins (12), and the cellular pool of deoxyribonucleotides (13–16). The ATR signaling pathway is also essential for the proliferation of cancer cells that display intrinsically higher levels of genotoxic stress. Therefore, several clinical trials are evaluating the efficacy of ATR inhibitors in patients with cancer (17), particularly cancers in which the oncogene CDC25A is overexpressed (18). However, as kinase inhibitors often exert a strong selective pressure for the acquisition of drug resistance through kinase mutations, alternative therapeutic options must be identified (19).

Unlike classical approaches that target the activity of a specific protein with small molecule inhibitors, recent cell biology advances suggest that targeting biomolecular condensates may provide conceptually novel approaches to drug discovery (20). Biomolecular condensates are subcellular compartments that selectively concentrate hundreds of proteins and nucleic acids, without a surrounding membrane (21,22). These structures underlie the spatiotemporal organization of multiple biological processes. Moreover, the aberrant properties of condensates have been implicated in many diseases, including neurodegeneration, cardiomyopathy, cancer and viral infections (20). Condensate formation is typically driven by multivalent scaffold proteins that function as central nodes in molecular networks (21,22). Therefore, one potential approach to disturb the condensate properties and functions is to interfere with their essential protein-protein or protein-nucleic acid interactions.

In humans, the main ATR activator in S phase is Topoisomerase IIβ binding protein 1 (TopBP1), a scaffold protein that includes nine BRCA1 carboxyl terminal (BRCT) protein-protein interaction motifs (23,24) and an intrinsically disordered ATR-activation domain located between BRCT6 and BRCT7-8 (23,25). Recent studies indicate that TopBP1 activates the ATR signaling pathway via the formation of biomolecular condensates, which appear as nuclear foci by immunofluorescence microscopy (26). The available evidence suggests that ATR activation is a multistep process (27,28). TopBP1 is recruited to ATR-activating DNA structures by MRE11 (29) and binds to RPA (30), ATRIP (31) and the 9-1-1 complex

(32,33) to form a stable ATR-activating complex. Then, TopBP1 is phosphorylated by the basal kinase activity of ATR, triggering the assembly of TopBP1 condensates (26). We found that TopBP1 condensation functions as a molecular switch that amplifies ATR activity up to the level required for signal transduction by the checkpoint effector kinase Chk1 (26).

Here, we explored the feasibility of targeting TopBP1 condensates as a novel strategy to interfere with ATR signaling and sensitize colorectal cancer (CRC) cells to chemotherapeutic drugs. We present a high throughput optogenetic screening approach to identify small-molecule modulators of TopBP1 condensation. Using this approach, we identified AZD2858, a known glycogen synthase 3β (GSK-3β) inhibitor, as a potential modulator of TopBP1 condensation. We demonstrated in a CRC cell line that AZD2858 (at very low doses) inhibits the assembly of endogenous TopBP1 and suppresses the activation of the ATR/Chk1 pathway induced by the topoisomerase I inhibitor SN-38, the active metabolite of irinotecan. Furthermore, the combination of AZD2858 with FOLFIRI (5-fluorouracil + SN-38) displayed a synergistic effect in CRC cell spheroid cultures, including in spheroids from CRC cells resistant to SN-38. Incubation with AZD2858 for 6-12 hours improved the induction of apoptosis by SN-38 and FOLFIRI by dampening the S checkpoint. Our observations suggest that the cytotoxic effects observed with the AZD2858 and SN-38 combination are mainly explained by disruption of TopBP1 assembly, rather than by the direct involvement of the GSK-3β pathway. These data supports the feasibility of targeting condensates formed in response to DNA damage to improve chemotherapy-based cancer treatments.

Materials and methods

Cell culture

Flp-In™ 293 T-REx cells were obtained from Thermo Fisher and cultured in Dulbecco's Modified Eagle Medium (DMEM)-GlutaMAX medium supplemented with 10% heat-inactivated fetal bovine serum (FBS). For the generation of stable cell lines that express TopBP1 fused to the photoreceptor cryptochrome 2 (Cry2) and mCherry (optoTopBP1), please refer to Egger et al., 2024 (28). The HCT116 human CRC cell line was obtained from Horizon (#HD-PAR-082) and cultured in RPMI (Merck-Sigma-Aldrich, #R8758) with 10% heat-inactivated FBS. The human SW620, SW480, HT29 and murine CT26 CRC cell lines, from ATCC, were grown in RPMI1640 medium (Gibco, #61870-010) with 10% FBS and 2 mmol/L L-glutamine. All cell lines were maintained at 37 °C in saturated humidity with 5% CO_2. The SN-38-resistant clones HCT116-SN6 (low-level resistance) and HCT116-SN50 (high-level resistance) were generated in the laboratory as previously described (34). Briefly, parental HCT116 cells were grown in the presence of 10 nmol/L or 15 nmol/L SN-38, respectively. SW620 shLuc and SW620 shGSK3-β cells were kindly given by Maguy Del Rio. The description of how they were generated is in Cherradi et al. 2023 (35). Add in what medium you cultured them.

All cell lines were tested and authenticated by short-tandem repeat profiling (Eurofins Genomics). Cells were routinely tested for mycoplasma contamination.

Drugs and antibodies

A personalized TargetMol library containing 4730 molecules was used for the high throughput screening (see Screening section). SN-38 (active metabolite of irinotecan, Tocris #2684) was diluted to 10 mM in DMSO and stored at -20 °C. 5-fluorouracil (5-FU; Sigma, #F6627) was diluted to 10 mM in water and stored at room temperature (RT). AZD2858 (Euromedex, #AB-M2178) was diluted to 10 mM in DMSO and stored at -80 °C. The drugs were diluted in the adapted medium and tested at the concentrations indicated in the figures.

The following primary antibodies were used: anti-Chk1 phosphorylated at S345 (Cell Signaling Technology, #2348), anti-ATR phosphorylated at T1989 (Abcam, #227851), anti-Chk2 phosphorylated at T68 (Cell Signaling Technology, #2661), anti-ataxia-telangiectasia mutated (ATM) phosphorylated at S1981 (Santa Cruz Biotechnology, #Sc47739), anti-p53 phosphorylated at S15 (Cell Signaling Technology, #9286), anti-p21 Waf1/Cip1 (Cell Signaling Technology, #2947), anti-DNA-dependent protein kinase catalytic subunit (DNA-PKcs) phosphorylated at S2056 (Abcam, #ab124918). The antibody against H2AX phosphorylated at S139 (Abcam, #ab195189) was conjugated to Alexa Fluor®

647. Secondary antibodies were: goat anti-rabbit IgG (H + L) AF568 (Thermo Fisher Scientific, #A11011) and goat anti-mouse IgG (H + L) AF488 (Thermo Fisher Scientific, #A11029).

Screening

OptoTopBP1-expressing Flp-In 293 T-Rex cells were seeded in a 384-well plate at a density of 10,000 cells/well in DMEM supplemented with 10% FBS and 2 µg/ml doxycycline and allowed to attach overnight. Then, cells were incubated with the TargetMol library compounds at the concentration of 10 µM for 2 h. From the 10 mM stock solutions in DMSO, each compound was diluted to 2 mM (intermediated dilution) before addition to the wells by automated pipetting. After incubation, cells were exposed to cycling pulses (4 s 'ON', 10 s 'OFF') of 488 nm blue light for 5 min. Cells were fixed immediately in 4% paraformaldehyde (PFA) (Euromedex, #15710-S) diluted in phosphate-buffered saline (PBS) for 15 min. Cells were rinsed with PBS twice and permeabilized in PBS/0.2% Triton X-100 for 10 min. Cells were rinsed in PBS twice and nuclei were counterstained with 1µg/mL Hoechst 33342 (Thermo Fisher Scientific, #62249). Imaging was performed with the Opera PHENIX system at the Montpellier Ressources Imagerie facility.

Western blotting

Whole cell extracts were obtained by lysing cells in RIPA buffer (50 mM Tris, 150 mM NaCl, 1% NP-40, 1% deoxycholate, 0.1% SDS, pH 8) on ice for 30 min. After sonication (40% amplitude, 3 cycles of 3 s sonication and 3 s resting), the protein amount was quantified using the Pierce™ BCA Protein Assay Kit (Thermo Fisher #23225). Laemmli buffer was added, and protein extracts were boiled at 95 °C for 5 min. 40 µg of protein samples were resolved on precast SDS-PAGE gels (4-15%, 7.5% and 10%) and transferred to nitrocellulose membranes using the Bio-Rad Trans-Blot Turbo transfer device. Membranes were saturated in 5% non-fat milk diluted in TBS (20 mM Tris, 150 mM NaCl , pH 7.4)/0.1 % Tween 20, and incubated with primary antibodies at 4°C overnight. The used antibodies were against Chk1 phosphorylated at S345 (Cell Signaling, #2348), Chk1 (Santa Cruz Biotechnology, #sc8408), Chk2 phosphorylated at T86 (Cell signaling #2661S), Chk2 (Milipore, #05-649), TopBP1 (Euromedex, #A300-111A or Santa-Cruz, #sc-271043), ATR phosphorylated at T1989 (Euromedex, #GTX128145), ATR (Bethyl/Euromedex, #A300-137A), ATM phosphorylated at S1981 (Rockland, #200-301-400), α-tubulin (Sigma, #T5168), H3 (Cell Signaling Technology, #4499S), vinculin (Merck, #V9131), γH2AX (Cell signaling, #9718S; Milipore, #05-636), RPA phosphorylated at S33 (Abcam, #ab2118877) and S4/8 (Euromedex, #A300-245A), RPA (Abcam, #AB2175), GSK-3β phosphorylated at S9 (Cell Signaling Technology, #9336), GSK-3β (Cell Signaling Technology, #9832), and DNA-PKcs phosphorylated at S2056 (Abcam, #ab18192). For more information, please refer to Table S4. Membranes were then incubated with anti-mouse (Cell Signaling, #7076S) or anti-rabbit HRP (Cell Signaling, #7074S) secondary

antibodies for 1 h. Revelation was carried out with ECL Clarity (BIO-RAD, #170-5061) or ECL select (BIO-RAD, #1705062) according to the manufacturer's instructions.

Immunofluorescence analysis

Cells were grown on coverslips and after incubation with the corresponding drugs (see above) for 2 h, the soluble fraction of cells was removed during the pre-extraction step in Cytoskeleton buffer "CSK" (PBS containing 0.2% Triton X-100) at 4 °C for 60 s. Cells were then fixed with 4% PFA/PBS at RT for 20 min. Non-specific epitopes were saturated with a blocking solution (5% BSA/PBS) at RT for 30 min. For immunostaining, anti-TopBP1 (Santa Cruz, #sc-271043, diluted at 1/100), anti-53BP1 (Cell Signaling, #4937S) or anti-PML (Santa Cruz, #sc-966, diluted at 1/300) primary antibodies and the anti-mouse coupled to fluorochrome (Invitrogen, #A-11011, diluted at 1/500) secondary antibody were diluted in blocking solution and incubated for 1 h or 45 min, respectively. Three 5-min washes between incubation steps were performed in PBS/0.1% Tween 20 at RT. Hoechst was used at 1 µg/mL for DNA staining and coverslips were mounted on slides with the Prolong Gold antifade reagent (Invitrogen, #P36930). Images were captured using a 63 X objective and a Zeiss AxioImager with ApoTome at the Montpellier Ressources Imagerie facility.

TurboID assay: pulldown of biotinylated proteins

Flp-In 293 T-Rex cells that express optoTopBP1 and grown to 75% of confluence were incubated with 2 µg/ml of doxycycline for 16 h. The next day, during the last 15 min of incubation with the indicated drugs, 500 mM of biotin was added. Cells were then washed with PBS and lysed in lysis buffer (50 mM Tris-HCl pH 7.5, 150 mM NaCl, 1 mM EDTA, 1 mM EGTA, 1% NP-40, 0.2% SDS, 0.5% sodium deoxycholate) supplemented with 1X complete protease inhibitor, 1X phosphatase inhibitor and 250 U benzonase. Lysed cells were incubated on a rotating wheel at 4°C for 1 h before sonication (40% amplitude, 3 cycles of 1 s sonication – 2 s resting) on ice. After centrifugation at 7750 rcf at 4°C for 30 min, cleared supernatants were transferred to new tubes and the total protein concentration was determined using the Bradford protein assay. For each condition, 1 mg of proteins was incubated with 100 µl of streptavidin-agarose beads on a rotating wheel at 4°C for 3 h. After centrifugation at 400 rcf for 1 min, beads were washed sequentially with 1 ml lysis buffer, 1ml wash buffer 1 (2% SDS in H_2O), 1 ml wash buffer 2 (0.2% sodium deoxycholate, 1% Triton X-100, 500 mM NaCl, 1 mM EDTA, and 50 mM HEPES, pH 7.5), 1 ml wash buffer 3 (250 mM LiCl, 0.5% NP-40, 0.5% sodium deoxycholate, 1 mM EDTA, 500 mM NaCl and 10 mM Tris pH 8) and 1 ml wash buffer 4 (50 mM Tris pH 7.5 and 50 mM NaCl). Bound proteins were eluted from the agarose beads with 80 µl of 2X Laemmli sample buffer and incubated at 95 °C for 10 min. Western blot analysis was performed as previously described to analyze the self-proximity of optoTopBP1 molecules.

***Xenopus laevis* egg extract assay**

Interphasic Low Speed Egg extracts (LSE) and demembranated sperm nuclei were prepared as previously described (Menut S et al 1999). LSE were then clarified by centrifugation at 20,000 rpm in an SW55Ti rotor for 20 min. Chromatin preparation was performed as described before (Aze et al; 2016). Briefly, demembranated sperm nuclei were added at a final concentration of 4000 nuclei per microliter to LSE supplemented with energy regeneration mix (200 µg/ml creatine phosphokinase, 200 mM creatin phosphate, 20 mM ATP, 20 mM $MgCl_2$, 2 mM EGTA) and cycloheximide (250 µg/ml). When indicated, LSE were pre-incubated with camptothecin (CPT), AZD2858, or DMSO (as control) for 5 min. The mixtures were incubated at 23◦C for the indicated times, then samples were diluted in EB buffer (100 mM KCl, 50 mM Hepes-KOH, 2.5 mM $MgCl_2$, supplemented with 0.25% NP40) and centrifuged over a 30% sucrose cushion. Purified chromatin pellets were washed once with EB buffer and recovered in Laemmli buffer for western blot analysis.

Cell cycle assay

Cell cycle profiling using 5-bromo-2'-deoxyuridine (BrdU)/propidium iodide (PI) was performed as previously described (Egger et al., 2022). Briefly, cells were pulsed with 10 µM BrdU for 15 min and fixed in ice-cold 70% ethanol. Cells were digested in 30 mM HCl, 0.5 mg/mL pepsin (37 °C, 20 min). DNA was denatured in 2 N HCl (RT, 20 min) and BrdU was immunodetected using the anti-BrdU clone BU1/75 in PBS/2% goat serum/0.5% HEPES/0.5% Tween 20 and revealed with a goat anti-rat Alexa Fluor 488 secondary antibody. DNA was stained with 25 µg/mL PI in PBS and cells were analyzed on a Gallios flow cytometer (Beckman Coulter) at the Montpellier Ressources Imagerie facility. 20,000 cells/sample were analyzed using the Kaluza software.

Detection of apoptotic cells with the sub-G1 assay

For visualization of sub-G1 apoptotic cells by flow cytometry, the "SubG1 Analysis Using Propidium Iodide" protocol developed by the UCL - London's Global University was used. Briefly, cells were collected and fixed in ice-cold 70% ethanol, followed by two washes in phosphate-citrate buffer (192 mM Na_2HPO_4, 4 mM citric acid, pH 7.8). Ribonuclease A (100 µg/ml in PBS) digestion was performed at 37 °C for 30 min. DNA was stained with PI (50 µg/ml in PBS) for 15 min. Cells were analyzed on a Gallios flow cytometer (Beckman Coulter) at the Montpellier Ressources Imagerie facility. 20,000 cells/sample were analyzed with the Kaluza software. Debris (low FSC/SSC) was kept and the sub-G1 fractions were calculated as the percentage of sub-G1 (<2N PI content) cells relative to the total number of events.

Pulse Field Gel Electrophoresis (PFGE)

Cells were collected and embedded in 0.5% agarose plugs (in PBS), at the exact concentration of $0.7x10^6$cells per plug. Plugs were incubated in lysis buffer (100 mM EDTA pH8, 0.2% sodium deoxycholate, 1% sodium lauryl sarcosine, 1 mg/ml proteinase K) at 37°C for 48h. Plugs were washed 3 times in wash buffer (20 mM Tris pH 8, 50 mM EDTA pH 8) and inserted in 0.9% agarose gel prepared in 0.5X TBE (from a 5X stock PanReac-AppliChem #A4228). Chromosomes were separated by pulsed-field gel electrophoresis for 23 h (Biometra Rotaphor 8 System, 23 h; interval: 30-5 s log; angle: 120-110 linear; voltage: 180-120 V log, 13°C). Then, gels were stained with ethidium bromide (0.5 µg/mL) for analysis.

2D cell growth inhibition assay

Cell growth was evaluated using the sulforhodamine B (SRB) assay, as described by Skehan et al., 1990 (36). Briefly, 500 cells/well were seeded in 96-well plates. After 24 h, cells were incubated with the indicated drug concentrations for 96 h. Cells were fixed in 10% trichloroacetic acid solution (Sigma, #T9159), rinsed in water and stained with 0.4% SRB (Sigma, #S9012) in 1% acetic acid (Fluka, #33209). Plates were washed three times with 1% acetic acid and fixed SRB was dissolved in 10 mmol/L Tris-Base solution (Trizma®base SIGMA, #T1503). The absorbance was read at 560 nm using a PHERAstar FS plate reader (BMG Labtech). Non-treated controls were used to normalize the cell growth inhibition values. The IC_{50} of drugs were determined graphically using the cell growth inhibition curves.

3D spheroid assay

For spheroid generation, 100 µL/well of cell suspensions at optimized densities (50 cells/well) were dispensed in ultralow attachment 96-well round-bottomed plates (Corning B.V. Life Sciences, #7007) and cultured at 37 °C, 5% CO_2, 95% humidity. Cells were first incubated with the indicated drugs at day 1 and then at day 4. At day 7, images were captured with the Celigo Imaging Cytometer (Nexcelom Bioscience) using the "Tumorosphere" application. Cell viability was measured using a CellTiter-Glo Luminescent Cell Viability Assay (Promega, #G9683), according to the manufacturer's instructions. Luminescence was measured in the white 96-well plates using a PHERAstar FS plate reader (BMG LABTECH). The IC_{50} was determined graphically from the cytotoxicity curves.

Synergy matrix

The percentage of living cells after incubation with each drug alone or in combination was calculated and normalized to that of untreated cells. Then, using a script developed by Tosi et al., 2018 (37) in the “R” software based on the effect of each molecule alone (Bliss and Lehàr equation), a synergy matrix was generated. This matrix associates a number to each drug combination: if positive (red), it indicates

synergistic effects; if negative (green), it indicates antagonistic effects. Additives effects (~ 0) are displayed in black.

In vitro cytotoxicity assays

Cells were seeded at 500 cells/well in black flat-bottom 96-well plates (Sarstedt, #83.3924), cultured for 24 h, then incubated with AZD2858 or/and FOLFIRI for 96 h. Then, PI (Sigma, #P4864) and Hoechst 33342 (Thermo Fisher Scientific, #62249) were added to the plates at the final concentrations of 1 and 5 µg/mL, respectively. Cells were incubated at 37 °C for 30 min before counting the positive cells for each fluorescence signal using a Celigo Imaging Cytometer (Nexcelom Bioscience) and the "Expression analysis – Cell Viability - Dead + Total" application. The number of living cells was then calculated by subtracting the number of dead, PI-positive cells, from the number of total cells given by the Hoechst staining. The percentages of live and dead cells were plotted and cytotoxic and cytostatic profiles were determined, as previously described by Vezzio-Vie et al., 2022 (38).

Celigo imaging cytometer-based immunofluorescence analysis

HCT116 cells were seeded at 1,200 cells per well for 48 h or 24 h in black 384-well plates (Greiner, #781091) and incubated with increasing concentrations of AZD2858 and/or FOLFIRI (diluted to 1/2, corresponding to 50 nM of SN-38 and 6 µM of 5-FU) for 2 and 20 h, respectively. Then, cells were fixed in 4% PFA, permeabilized in PBS/0.1% Triton X100 (Sigma), and saturated in 3% BSA/PBS. The primary anti-Chk1 phosphorylated at S345 antibody (Cell Signaling Technology, #2348L) was diluted (1/50) in 1% BSA/PBS and cells were incubated at 4 °C under stirring overnight. Cells were washed three times with 0.05% Tween 20/PBS (Tween®20 Polysrobate Technical VWR CHEMICALS). The Alexa Fluor 568 goat anti-rabbit IgG (H + L) (Thermo Fisher Scientific, #A11011) secondary antibody was added at RT for 45 min. The anti-γH2AX (phosphorylated at S139) (Abcam, #195189) antibody was diluted (1/1000) in 1% BSA/PBS and added to the cells at RT for 45 min. Cells were washed three times and 1 µg/mL of Hoechst 33342 in PBS was used to counterstain nuclei (37 °C, 30 min). Fluorescence signals were acquired using the “Expression analysis – Target 1 + Mask” application on the Celigo Imaging Cytometer (Nexcelom). The percentage of positive cells, the mean signal intensity per well, and the total cell count were calculated using the Nexcelom Bioscience Celigo Satellite software.

DNA fiber assay

$1x10^6$ HCT116 cells were seeded in 6-well plates. Cells were allowed to attach overnight and then sequentially pulsed with 20 µM 5-iodo-2’-deoxyuridine (IdU) (20 min) and 200 µM 5-chloro-2’-deoxyuridine (CldU) (20 min). Cells were harvested, washed and diluted in ice-cold PBS to 0.5–1×10^6 cells/mL. 2 µL of cell suspension was pipetted on the edges of SuperFrost microscopy slides.

After drying at RT for 3–5 min, 7 µL of DNA Spreading Buffer (200 mM Tris–HCl pH 7.5, 50 mM EDTA, 0.5% SDS) was mixed with the cell-containing drops. After drying at RT for 2–5 min, slides were manually tilted (15 ° – 30 °) to spread the DNA fibers that were then fixed in a 3:1 methanol/acetic acid solution at RT for 10 min. Slides were washed in H_2O and DNA was denatured in 2.5 M HCl for 1 h. Slides were washed and blocked in PBS/1% BSA/0.1% Tween 20 at RT for 1 h. Then, slides were incubated with a mix of anti-IdU (BD Biosciences, Cat# 347580; RRID:AB_10015219) and anti-CldU (Bio-Rad, Cat# OBT-0030, RRID:AB_2314029) antibodies, both diluted (1/25) in PBS/0.1% Tween 20, at 37 °C in saturated humidity for 45 min. Slides were washed in PBS/0.1% Tween 20 five times (2 min/each) and incubated with a mix of secondary antibodies, diluted 1/50 in PBS/0.1% Tween 20, at 37°C for 30 min. Slides were rinsed in PBS/0.1% Tween 20 five times (2 min/each), dried and mounted with 24 × 50 mm coverslips in 30 µL of ProLong Gold Antifade. Twenty representative pictures for each condition were saved on a Zeiss Axio Imager (40 X objective). The CldU tract lengths of individual fibers consisting of a sequence of IdU and CldU tracts were measured using the open source FiberQ software (39). Experiments were repeated three times and the pooled data from three replicates were plotted using the online tool SuperPlotsOfData (40). The non-parametric unpaired Mann–Whitney test was used to determine the significance of the results.

Software tools

Immunofluorescence data were acquired with a Zeiss AXIOIMAGER microscope (Zeiss) and the Zen toolkit connect software. For foci quantification, the pipelines generated on CellProfiler 4.2.1 and described in Egger et. Al, 2024 were used. For western blot images acquisition, ChemiDoc Imaging System (Biorad) and ImageLab 6.1 were used. The R studio software was used to generate the synergy and viability matrixes with a predefined script. GraphPad version 8 was used for graphical representation and statistical analyses. R was used for statistical analyses. The DNA fibers were quantified using open source FiberQ software.

Statistical analyses

For the immunofluorescence and DNA fiber analyses, groups were first compared using one-way ANOVA and confirmed using non-parametric unpaired Mann-Whitney tests on GraphPad Prism version 10.2.1 (the non-normal distributions of foci limited the precision of the ANOVA analyses). For cytometric analyses, linear regression analysis was performed on R. For the Celigo data quantifications, after assessing the normality of data distribution, the Student's *t*-test was used to compare experimental replicates with GraphPad Prism version 8. In all cases, significance thresholds were as follows: ns: non-significant; $*p < 0.05$; $**p < 0.01$; $***p < 0.001$; $****p < 0.0001$.

For analysis of TopBP1 foci in parental and SN-38-resistant HCT116 cells, biological replicates were pooled and plotted using SuperPlotsOfData (https://huygens.science.uva.nl/SuperPlotsOfData/) (41). Data distribution was displayed as half-violin plots on the right-hand side of the dot plots to help data visualization. Detailed R scripts and data files for the analysis of data shown in Figures 2A, 2C, 3B, 4B, S1 and S3 are available at https://github.com/HKeyHKey/Morano_2025.

Results

Identifying modulators of TopBP1 condensation with an optogenetic approach

Resistance to conventional chemotherapies is the major cause of therapy failure in patients with cancer. In CRC, irinotecan resistance is often caused by overexpression of efflux pumps (42). However, additional pathways may also contribute, particularly the DNA damage response pathways that are frequently activated in various cancer types to cope with increased DNA replication stress. TopBP1 has been implicated in oxaliplatin resistance in gastric cancer (43) and is overexpressed in several cancer types (44). We first examined the number of TopBP1 condensates in the CRC lines HCT116 and HCT116-SN50 (50-fold more resistant to SN-38, the active metabolite of irinotecan, than the parental HCT116 cell line) (45) and observed a significantly higher number of TopBP1 foci in HCT116-SN50 cells (**Figure S1**). Moreover, our previous findings suggest that TopBP1 condensation is required to amplify ATR activity (26). Therefore, targeting TopBP1 assembly could be a promising strategy for cancer treatment. To this end, we developed an optogenetic system for screening molecules that modulate the formation of TopBP1 condensates. We used the stable Flp-In 293 T-Rex cell line in which expression of TopBP1 fused to the photoreceptor Cry2 and mCherry (optoTopBP1) is induced by doxycycline. Cry2 forms tetramers when exposed to 488 nm light and thereby nucleates the assembly of TopBP1 condensates (26). The advantage of this optogenetic approach is that TopBP1 condensates are formed on demand, within minutes, in the absence of DNA damaging agents that can induce confounding effects after prolonged treatment. After a 2-hour incubation step of optoTopBP1-expressing Flp-In 293 T-Rex cells with 10 µM of each molecule from the TargetMol library of preclinical and clinical compounds, we exposed cells to an array of blue light-emitting diodes for 5 min of light-dark cycles (4 s light followed by 10 s dark) to induce optoTopBP1 condensation (**Figure 1A**). After quantification of the number of TopBP1 foci per nucleus, we assigned a z-score to each candidate molecule based on this count. We considered molecules with a z-score lower than -2 as potential TopBP1 condensation inhibitors (red dots in **Figure 1B**). We identified >300 molecules that could be potential TopBP1 condensation inhibitors among the 4730 compounds. Then, we selected 131 compounds (based on the best z-scores) and assessed their effect on the ATR pathway activation in HCT116 cells using two complementary

approaches. First, we evaluated these compounds at two low concentrations (1 and 10 µM) using a quantitative immunofluorescence assay (46) in flat-bottomed 384-well plates to monitor phosphorylation at S315 of the kinase effector Chk1 following incubation with SN-38 alone or with each of the 131 pre-selected compounds (**Figure 1C**). This allowed us to select the ten most effective drugs (MCB-613, OTSSP167, AZD2858, P005091, tubercidin, dactolisib, physalin F, PFK158, PF562271, TORKINIB) based on their ability to inhibit Chk1 phosphorylation. For the second approach, we incubated HCT116 cells with 5-FU and SN-38 (FOLFIRI thereafter) to mimic *in vitro* the first-line chemotherapy regimen for patients with metastatic CRC (i.e., FOLFIRI: folic acid or leucovorin, 5-FU, and irinotecan) and each of the ten drugs and detected their interactions using a full-range dose matrix approach and SRB cytotoxicity assays. We quantified cell survival and the additive, synergistic or antagonistic effects. We observed the strongest synergistic interactions between FOLFIRI and AZD2858 (a known GSK-3β inhibitor). Consequently, we focused our study on AZD2858, which was efficient already at 1 µM (**Figure 1D**).

Figure 1. Identification of TopBP1 condensation inhibitors by high throughput screening. ***(Next page)***
(**A**) Schematic description of the high-throughput screening system. Doxycycline-inducible TopBP1 was fused to mCherry and the light-sensitive cryptochrome 2 (Cry2) at its C-terminus and stably integrated in Flp-In 293 T-Rex cells. A 5-min blue light exposure (cycles of 4 s on and 10 s off) allows inducing optoTopBP1 condensation in the absence of DNA damage. Cells were grown in 384-well plates, incubated with 10 µM TargetMol molecules for 2 h before inducting optoTopBP1 condensate formation. (**B**) Graphical representation of the screening results. Drugs with a z-score lower than -2 were considered inhibitors, and drugs with a z-score higher than 2 were considered activators of TopBP1 condensate formation. The screening was performed in triplicate and each dot represents the mean z-score of a molecule. (**C**) Graphical representation of the screening confirmation in HCT116 cells. Chk1 phosphorylation at S345 was assessed using Celigo® immunofluorescence imaging after a 2-h co-incubation with SN-38 and each of the 131 drugs selected from the first screening. Drugs leading to Chk1 phosphorylation (pChk1) inhibition (>1.5-fold change) were considered promising candidates and the ten molecules leading to the highest inhibition were selected for the next screening. (**D**) Viability and synergy matrices obtained after HCT116 cell incubation with increasing concentrations of FOLFIRI (5FU from 0.009 to 0.148 µM, SN38 from 0.077 to 1.235 nM) and each of the ten drugs (MCB-613 13.3 to 850 nM, OTSSP167 7.8 to 500 nM, AZD2858 13.3 to 850 nM, P005091 31.5 to 1000 nM, tubercidin 0.15 to 10 nM, dactolisib 1.58 to 100 nM, physalin F 6.25 to 400 nM, PFK158 1.2 to 300 nM, PF562271 1.2 to 300 nM, TORKINIB 0.4 to 300 nM) for 96 h. Cell viability was assessed with the SRB assay. Blue matrices represent cell viability. The black/red/green matrices represent additivity/synergy/antagonism, respectively. The synergy matrices were calculated with an R script (see Materials and Methods).

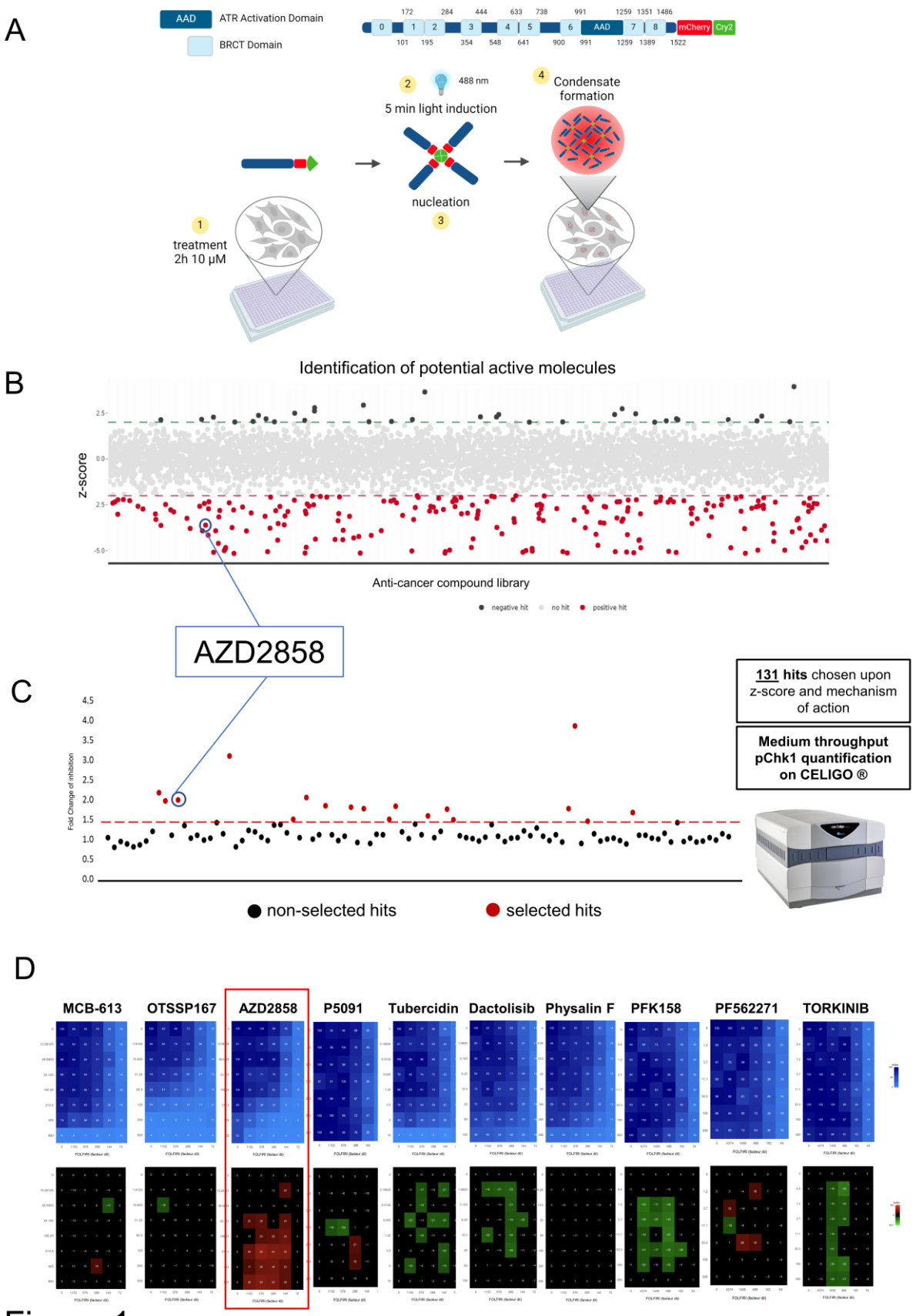

Figure 1

AZD2858 hampers SN-38-induced endogenous TopBP1 condensate formation and ATR activation

We then evaluated AZD2858 capacity to modulate endogenous TopBP1 condensation in HCT116 cells. To this aim, we induced TopBP1 condensation by incubating cells with 300 nM SN-38 or/and 100 nM AZD2858 for 2 h. Co-incubation with AZD2858 resulted in a significant reduction in the number of endogenous TopBP1 condensates per nucleus (**Figure 2A**). Co-incubation with AZD2858 also led to a decrease in the number of 53BP1 foci (**Figure S2A**). 53BP1 forms biomolecular condensates (47) and might interact with TopBP1 (48,49). Conversely, co-incubation with AZD2858 did not modulate the number of PML nuclear bodies, which are membrane-less organelles (**Figure S2B**). We then evaluated the effect of incubation of HCT116 cells with AZD2858 or/and SN-38 for 2 hours on ATR signaling (TopBP1 target) and on two other phosphoinositide 3-kinase-related protein kinases: ATM and DNA-PKcs. Western blot analysis showed that SN-38-mediated ATR signaling induction was severely reduced by co-incubation with 100 nM AZD2858, as indicated by the decrease in Chk1 phosphorylated at S345, and RPA32 phosphorylated at S33 (**Figure 2B**). We obtained a similar result for Chk1 phosphorylated at S345 using the Celigo cytometer in cells incubated with AZD2858 and FOLFIRI (**Figure 2C**). Co-incubation of AZD2858 with SN-38 or FOLFIRI did not affect the ATM and DNA-PKcs signaling pathways, as indicated by the unchanged levels of ATM phosphorylated at S1981 and Chk2 phosphorylated at T68 (ATM pathway) and of RPA32 phosphorylated at S4/8 and DNA-PKcs phosphorylated at S2056 (DNA-PKcs pathway) (**Figure 2B and Figure S3A**). DNA-PKcs phosphorylation level was significantly increased upon co-incubation with AZD2858 and FOLFIRI (**Figure S3A**). The level of γH2AX, a marker of DNA damage, was not affected by co-incubation with AZD2858 and SN-38 (or FOLFIRI) compared with SN-38 (or FOLFIRI) alone (**Figure 2B-C).** We obtained similar results (i.e. decrease in Chk1 phosphorylated at S345 and unchanged γH2AX levels) after co-incubation with FOLFIRI+AZD2858 for 20 hours (**Figure S3B**). Altogether, these findings suggest that AZD2858 significantly affects the ATR/Chk1 signaling pathway by inhibiting the assembly of TopBP1 condensates induced by the DNA-damaging agent SN-38.

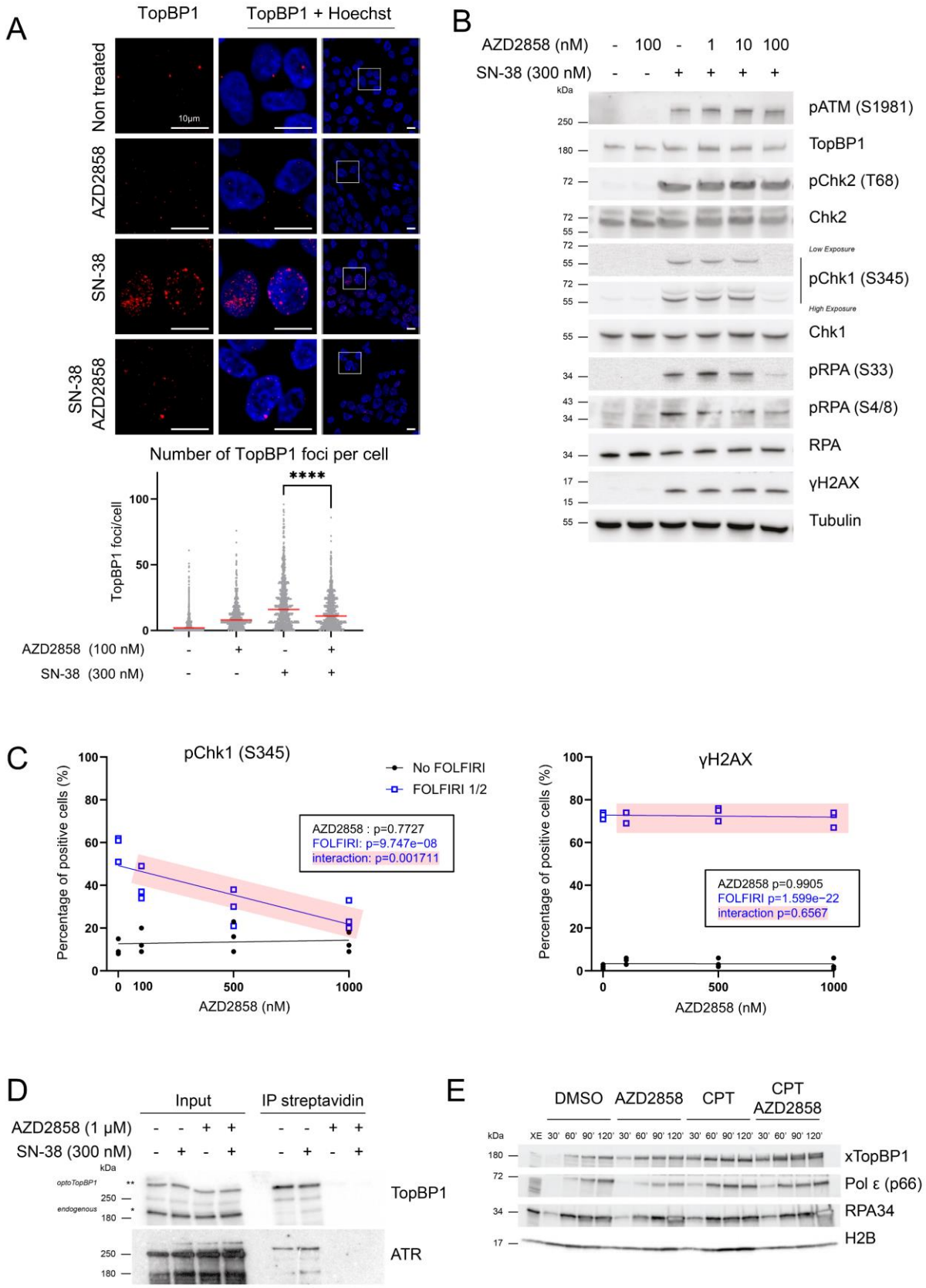
A
TopBP1
TopBP1 + Hoechst
Non treated
AZD2858
SN-38
SN-38 AZD2858
10µm
Number of TopBP1 foci per cell
****
TopBP1 foci/cell
AZD2858 (100 nM)
SN-38 (300 nM)
B
AZD2858 (nM) - 100 - 1 10 100
SN-38 (300 nM) - - + + + +
kDa
pATM (S1981)
TopBP1
pChk2 (T68)
Chk2
Low Exposure
pChk1 (S345)
High Exposure
Chk1
pRPA (S33)
pRPA (S4/8)
RPA
γH2AX
Tubulin
C
pChk1 (S345)
No FOLFIRI
FOLFIRI 1/2
AZD2858 : p=0.7727
FOLFIRI: p=9.747e−08
interaction: p=0.001711
Percentage of positive cells (%)
AZD2858 (nM)
γH2AX
AZD2858 p=0.9905
FOLFIRI p=1.599e−22
interaction p=0.6567
D
Input
IP streptavidin
AZD2858 (1 µM)
SN-38 (300 nM)
optoTopBP1
endogenous
TopBP1
ATR
E
DMSO
AZD2858
CPT
CPT AZD2858
XE 30' 60' 90' 120'
xTopBP1
Pol ε (p66)
RPA34
H2B

Figure 2

Figure 2. AZD2858 inhibits the formation of endogenous TopBP1 condensates and the ATR/Chk1 signaling pathway.

(**A**) Representative immunofluorescence images (upper panels) of TopBP1 biomolecular condensates in HCT116 cells incubated with AZD2858 (100 nM) or/and SN-38 (300 nM) for 2 h, and the corresponding quantification (lower panel). Scale bars, 10 µm. The experiment was replicated 3 times. Cell profiler was used for quantifying TopBP1 foci (>1000 cells analyzed per condition). ANOVA analysis of a generalized linear model (modeling TopBP1 foci number with a Poisson distribution) shows that SN38 and AZD2858 treatments exhibit significantly negative interaction on TopBP1 foci number (SN38 treatment *p*-value<2.2e-16; AZD2858 treatment *p*-value<2.2e-16; SN38:AZD2858 interaction *p*-value<2.2e-16). (**B**) Immunoblot of the indicated proteins after incubation of HCT116 cells with AZD2858 at the indicated concentrations and/or SN-38 (300 nM) for 2 h. The experiment was replicated 3 times, and a representative replicate is shown. (**C**) Percentage of HCT116 cells positive for phosphorylated Chk1 (S345) or γH2AX expression in function of the AZD2858 concentration (0 nM, 100 nM, 500 nM, 1000 nM) in the presence (blue) or not (black) of FOLFIRI (dilution: 1/2, corresponding to 6 µM of 5-FU and 50 nM of SN-38). Cells were incubated for 2 h and positive cells were identified using Celigo® immunofluorescence imaging. The experiment was replicated 3 times, and each point represents a biological replicate. The statistical significance was determined by linear modeling interrogating the effect of each drug separately and their interaction (*p*-values given in the inset). (**D**) Immunoblotting of TopBP1 and ATR isolated with streptavidin beads from optoTopBP1-expressing cells incubated with doxycycline for 16 h to induce optoTopBP1 expression, and also with AZD2858 (1 µM) and/or SN-38 (300 nM) for the last 2 h. Biotin was added to the medium in all conditions for the last 30 min. Bands that correspond to endogenous and optoTopBP1 proteins are indicated with one and two stars (* and **), respectively. The experiment was replicated twice, and a representative result is shown. (**E**) Chromatin was extracted at the indicated time points (min) following the assembly of nuclei from sperm DNA incubated in *X. laevis* egg extracts incubated with DMSO (control), camptothecin (CPT; 55 µM) or/and AZD2858 (1 µM). Chromatin samples were analyzed by western blotting.

AZD2858 modulates ATR/Chk1 signaling by disrupting TopBP1 assembly

As AZD2858 is a known GSK-3β inhibitor, we asked whether its effects on the ATR/Chk1 signaling pathway might be mediated by inhibiting the GSK-3β pathway. We incubated SW620 cells in which endogenous GSK-3β was depleted or not by shRNA with SN-38 or/and AZD2858 (0.1 and 1 µM) for 2 hours. SN-38-induced Chk1 phosphorylation at S345 was comparable in GSK3-β-depleted cells (shGSK3) and control cells (shLuc) (**Figure S4A**). Moreover, the SN-38+AZD2858 combination inhibited Chk1 phosphorylation in shGSK3 and shLuc cells, indicating that GSK-3β is not involved in Chk1 phosphorylation inhibition by AZD2858. The combination did not increase significantly the level of GSK-3β phosphorylated at S9, a marker of kinase inhibition, unlike what observed with insulin, a well-known regulator of GSK-3β activity (50) (**Figure S4B**). In addition, among the molecules tested from the TargetMol library, other more effective and specific GSK-3β inhibitors, compared with AZD2858, did not show any effect on light-induced optoTopBP1 condensation (**Table S1**). These findings suggest that although AZD2858 is a GSK-3β inhibitor, its modulation of the ATR/Chk1 pathway is not due to this function. To identify the underlying mechanisms, we used a biotin proximity-labeling approach to assess TopBP1 interaction with cellular partners in the presence of AZD2858 or/and SN-38 (51). For this, we used our optoTopBP1 construct tagged at its N-terminus with TurboID, an optimized biotin

ligase that allows protein biotinylation within minutes (52). We incubated Flp-In 293 T-Rex cells that stably express TurboID-tagged optoTopBP1 with AZD2858 or/and SN-38 for 2 hours and added biotin for the last 30 minutes. Isolation of biotinylated proteins using streptavidin-coated beads highlighted a drastic reduction in TopBP1 condensate formation with recombinant and endogenous TopBP1 and also with ATR upon incubation with AZD2858 alone or with SN-38 (**Figure 2D**). These findings suggest that AZD2858 disrupts TopBP1 self-association and its interaction with its primary activator ATR. This may contribute to the observed decrease in SN-38-induced TopBP1 foci following AZD2858 administration. Next, we determined whether TopBP1 recruitment to chromatin was altered by AZD2858 using the well-established cell-free DNA replication system derived from *X. laevis* egg extracts in which replication of demembranated sperm nuclei occurs synchronously, independently of transcription or protein synthesis. In the presence of the topoisomerase I inhibitor CPT, replication fork progression was challenged and polymerase (Pol) ε level was decreased and DNA-bound TopBP1 and RPA accumulated for the checkpoint response activation (**Figure 2E**). When AZD2858 was added to the extract alone or with CPT, TopBP1 recruitment to chromatin was not inhibited. We observed an increased in RPA, TopBP1 and Pol ε levels when CPT and AZD2858 were are added together. This may be due to increased origin activation, as normally seen when the S-phase checkpoint is inhibited (53). Collectively, these observations suggest that AZD2858 acts primarily on the ATR signaling pathway through TopBP1 self-association inhibition.

AZD2858 inhibits induction of the S-phase checkpoint by SN-38

Chk1 plays a pivotal role as a mediator of the S-phase checkpoint (54). As SN-38-induced phosphorylation of Chk1 was decreased after incubation with AZD2858, we investigated the impact of SN-38 or/and AZD2858 on the cell cycle by incubation with BrdU for 2 hours. BrdU incorporation was markedly reduced in SN-38-treated HCT116 cells, suggesting a slowdown of the S phase. However, when SN-38 was combined with AZD2858, this effect was reduced (red arrows in **Figure 3A**). To determine whether this depended on replication fork progression or replication origin firing, we co-labeled replication tracks with two consecutive pulses of the thymidine analogs IdU and CldU (**Figure 3B**). As expected, CldU tracks were shorter in HCT116 cells incubated with SN-38 alone, while addition of AZD2858 significantly reduced the negative impact of SN-38 on replication fork progression. Furthermore, prolonged co-incubation with AZD2858 for 6 and 12 hours effectively abolished the SN-38 induced S-phase checkpoint (**Figure 3C**). Specifically, BrdU incorporation increased from 16.11% (SN-38 alone) to 41.83% (combination) at 6 hours and from 20.87% (SN-38 alone) to 34.07% (combination) at 12 hours (**Figure 3C and S5A-B left panels**). These results indicate that the combination of

AZD2858+SN-38 affects replication fork progression and disrupts the cell cycle homeostasis, likely by inhibiting the ATR/Chk1 signaling pathway.

Egger et al, showed that in HCT116 cells, DNA-PKcs triggers a post-replicative cell cycle checkpoint in response to SN-38 combined with ATR inhibition (55). Therefore, we followed cell cycle progression by pulse-chasing HCT116 cells with BrdU for 15 minutes before incubation with SN-38 or/and AZD2858 for 6 and 12 hours. We observed a progressive accumulation of BrdU-positive cells with 4N DNA content: 8.5% at 6 hours and 8.86% at 12 hours in cultures co-incubated with SN-38 and AZD2858 and 6.15% at 6 hours and 4.71% at 12 hours in cells incubated with SN-38 alone (**Figure S5B**). This suggests that the combination of SN-38 and AZD2858 attenuates the S-phase checkpoint, thereby activating a compensatory post-replicative cell cycle checkpoint that arrests the cell cycle before mitosis in a DNA-PKcs-dependent manner. Abrogation of the replication checkpoint allows cells to enter the S phase with unrepaired DNA damage. We evaluated the level of DNA double-strand breaks (DSBs) using PFGE and monitored γH2AX and cleaved PARP1 expression by western blotting in cells exposed to SN-38 and AZD2838 at various time points. DSBs remained elevated after the combined treatment (**Figure 3D**). Additionally, γH2AX and cleaved PARP1 levels increased at later time points of incubation (**Figure 3E**). We noticed a modest increase in the level of DNA-PKcs phosphorylated at S2056, which is required for DSB repair via the non-homologous end-joining pathway (**Figure 3E**). Altogether, these findings indicate that the AZD2858+SN-38 combination disrupts TopBP1 assembly, most likely by inhibiting ATR kinase activity amplification, a critical process for inducing the S-phase checkpoint and regulating DNA damage repair.

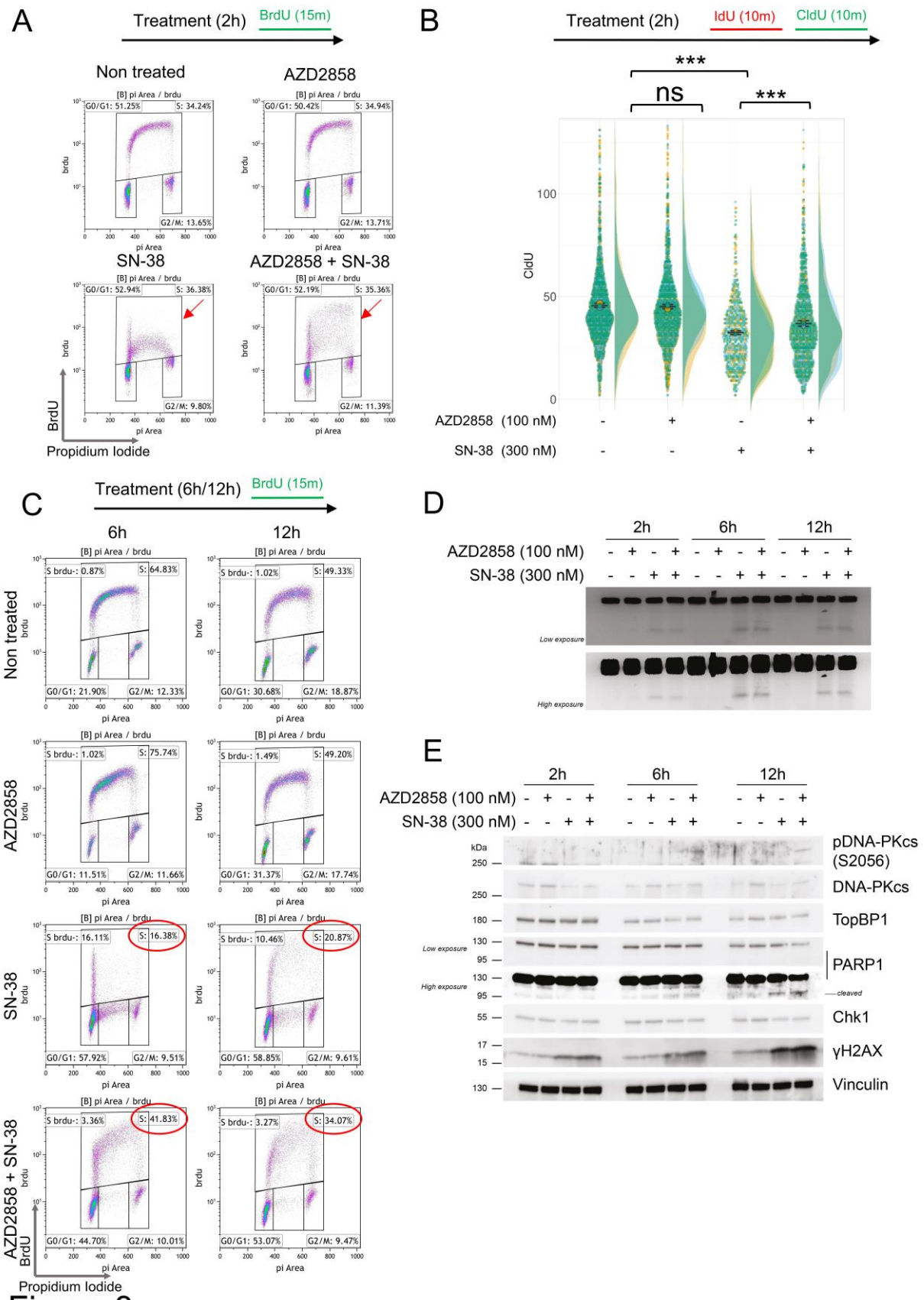
A
Treatment (2h)
BrdU (15m)
Non treated
AZD2858
SN-38
AZD2858 + SN-38
BrdU
Propidium Iodide
B
Treatment (2h)
IdU (10m)
CldU (10m)
***
ns
***
CldU
AZD2858 (100 nM)
SN-38 (300 nM)
C
Treatment (6h/12h)
BrdU (15m)
6h
12h
Non treated
AZD2858
SN-38
AZD2858 + SN-38
BrdU
Propidium Iodide
D
2h
6h
12h
AZD2858 (100 nM)
SN-38 (300 nM)
Low exposure
High exposure
E
2h
6h
12h
AZD2858 (100 nM)
SN-38 (300 nM)
kDa
pDNA-PKcs (S2056)
DNA-PKcs
TopBP1
PARP1
cleaved
Chk1
γH2AX
Vinculin
Low exposure
High exposure

Figure 3

Figure 3. AZD258 inactivates the S-phase checkpoint in SN-38-treated cells.
(**A**) Cell cycle analysis after a 2-h incubation with AZD2858 (100 nM) and/or SN-38 (300 nM); 10 µM BrdU was added in the last 15 min of the 2-h incubation. Cell debris were gated out and BrdU incorporation was plotted against DNA content (stained with PI). Red arrows indicate BrdU incorporation. 20,000 events per condition were analyzed. The G_0/G_1, S and G_2/M gates are shown. The experiment was replicated 3 times, and a representative replicate is shown. (**B**) DNA fiber analysis of replication tracts labeled with two sequential 15-min pulses of IdU and CldU added at the end of the 2-h incubation with AZD2858 (100 nM) +/- SN-38 (300 nM). The dot plots show the CldU tract length of individual replication forks. Data are pooled from n = 3 biological replicates (yellow, blue, green). Data distribution is shown as half-violin plots. Circles represent the mean of each replicate, and the error bars represent the SEM of the means of the three replicates. ANOVA analysis of a generalized linear model (modeling replication tract length with a gamma distribution) shows that both drugs, as well as their interaction, have a significant effect on tract length (p-value for SN38 treatment: < 2.2e-16; for AZD2858 treatment: 0.01129; for their interaction: 2.651e-06). We did not detect a significant effect of replicate identity (p-value=0.26274). (**C**) Same as (A) but after 6 h or 12 h of incubation with AZD2858 (100 nM) and/or SN-38 (300 nM). The gate of interest (S-phase) and the corresponding cell percentages are outlined in red. (**D**) PFGE analysis of DNA damage in HCT116 cells incubated with AZD2858 (100 nM) and/or SN-38 (300 nM) for the indicated times. The experiment was replicated 3 times, and a representative replicate is shown. (**E**) Immunoblot of the indicated proteins after incubation with AZD2858 (100 nM) or/and SN-38 (300 nM) for the indicated times. The experiment was replicated 3 times, and a representative replicate is shown.

AZD2858 treatment synergizes with classic chemotherapy drugs

In the absence of an effective S-phase checkpoint, DNA damage can lead to apoptosis and cell death. To assess this, we stained HCT116 cells with PI and quantified the sub-G1 population to measure cell death. After 48-hour incubation with sub-lethal doses of SN-38 and AZD2858, the sub-G1 cell population was increased by 40% compared with untreated cells, indicative of apoptotic cells (**Figure 4A**) and consistent with the early increase of cleaved PARP1 (**Figure 3E**). We obtained the same results in cells incubated with AZD2858 and FOLFIRI. Specifically, the sub-G1 population increased from 19.18% after incubation with SN-38 alone to 60.70% after incubation with SN-38+AZD2858, and from 27.19% after incubation with FOLFIRI alone to 70.67% after incubation with FOLFIRI+AZD2858 (**Figure 4A-B**). Additionally, the combined treatments (AZD2858 with SN-38 or FOLFIRI) led to an increase of cleaved PARP1 and cleaved caspase-3 (western blotting, **Figure 4C**), and to the accumulation of DNA DSBs (PFGE, **Figure 4D**). Then, we performed an SRB assay in HCT116 cells incubated with the AZD2858+SN-38 combination, as previously described, and visualized the viability (blue) and synergy (black/red) matrices. The AZD2858+SN-38 combination, like the AZD2858+FOLFIRI combination (**Figure 1D**), synergistically inhibited cell survival (**Figure 4E**).

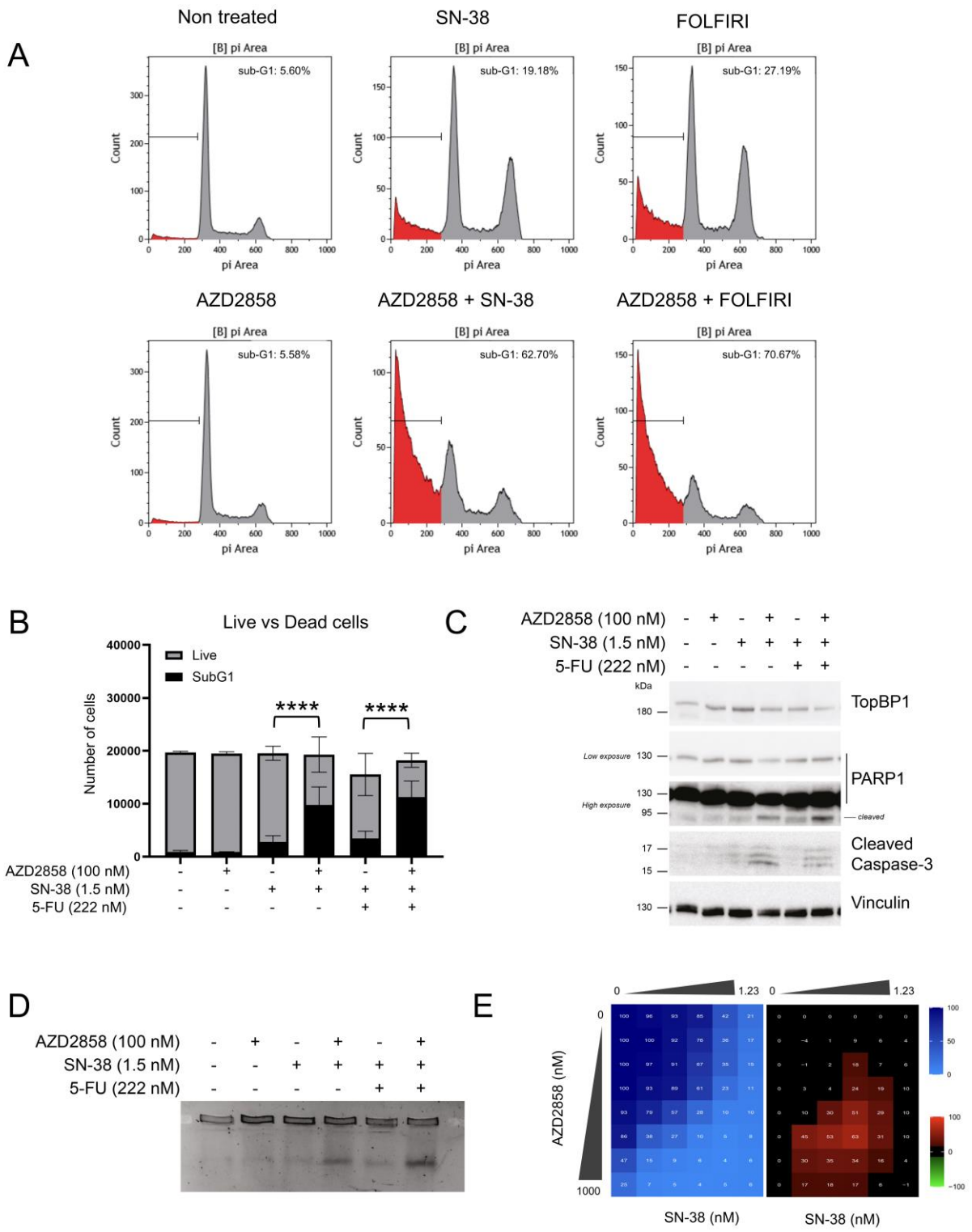
A
Non treated
SN-38
FOLFIRI
AZD2858
AZD2858 + SN-38
AZD2858 + FOLFIRI
[B] pi Area
sub-G1: 5.60%
sub-G1: 19.18%
sub-G1: 27.19%
sub-G1: 5.58%
sub-G1: 62.70%
sub-G1: 70.67%
Count
pi Area
B
Live vs Dead cells
Live
SubG1
Number of cells
****
****
AZD2858 (100 nM)
SN-38 (1.5 nM)
5-FU (222 nM)
C
AZD2858 (100 nM)
SN-38 (1.5 nM)
5-FU (222 nM)
kDa
TopBP1
Low exposure
PARP1
High exposure
cleaved
Cleaved Caspase-3
Vinculin
D
AZD2858 (100 nM)
SN-38 (1.5 nM)
5-FU (222 nM)
E
AZD2858 (nM)
SN-38 (nM)
SN-38 (nM)

Figure 4

Figure 4. AZD2858 synergizes with SN-38 and FOLFIRI by inducing DNA damage and cell apoptosis.
(**A**) Flow cytometry analysis to quantify sub-G1 HCT116 cells after 48-h incubation with sub-optimal doses of AZD2858 (100 nM) alone or with SN-38 (1.5 nM) or FOLFIRI (SN-38 1.5 nM; 5-FU 222 nM). The x-axis shows the DNA content (PI staining) and the y-axis the cell count. The presence of sub-G1 cells gated under the G1 peak suggests DNA fragmentation, a characteristic feature of apoptotic cell death. The experiment was replicated 3 times, and a representative replicate is shown. (**B**) Graph showing the number of sub-G1 cells (considered as dead cells) versus the number of live cells, according to the indicated treatments (from A). Error bars represent 3 individual biological replicates. The statistical significance was determined by linear regression analysis, more information is available in **Table S2** (***: $p<0.0001$). (**C**) Immunoblot of the indicated proteins in HCT116 cells after 48-h incubation as described in A. (**D**) PFGE analysis of DNA damage in HCT116 cells incubated for 48 h as described in A. (**E**) HCT116 cells were incubated with increasing concentrations of SN-38 (0 to 1.23 nM) and AZD2858 (0 to 1000 nM) for 96 h (2D culture system). Cell viability was assessed with the SRB assay. The synergy matrix was calculated as described in Materials and Methods. The experiment was replicated 3 times, and a representative replicate is shown.

Next, we assessed whether the combination affected cell death or proliferation. First, we determined whether AZD2858, SN-38, and FOLFIRI alone induced cytotoxic (cell death) or cytostatic (inhibition of cell proliferation) effects by PI/Hoechst labeling of cells incubated with increasing concentrations of each drug. The three drugs displayed mainly cytostatic effects **(Figure 5A)**, as indicated by the absence of cell death (lower panels) even at doses that decreased cell proliferation (upper panels). Next, we stained with PI/Hoechst and performed SRB assays in HCT116 cells and CT-26 cells (murine CRC cell line) incubated with increasing concentrations of AZD2858 and FOLFIRI (matrix analysis). We found that the combination was cytostatic at low drug doses and became cytotoxic at higher doses **(Figure 5D and 5E)**, especially in areas where we detected synergy **(Figure 5B and 5C).** These results indicate that when the AZD2858+FOLFIRI combination shows synergistic effects, this interaction is cytotoxic. We confirmed the synergy of the FOLFIRI+AZD2858 combination in three additional human CRC cell lines: HT29, SW620 and SW480 **(Figure 5F)**. We also performed a matrix analysis in two SN-38-resistant cell lines: HCT116 SN-6 and HCT116 SN-50 (56) **(Figure 5G)**. The FOLFIRI+AZD2858 combination was synergistic in both SN-38-resistant cell lines, indicating that this combination may overcome drug resistance in colorectal cancer.

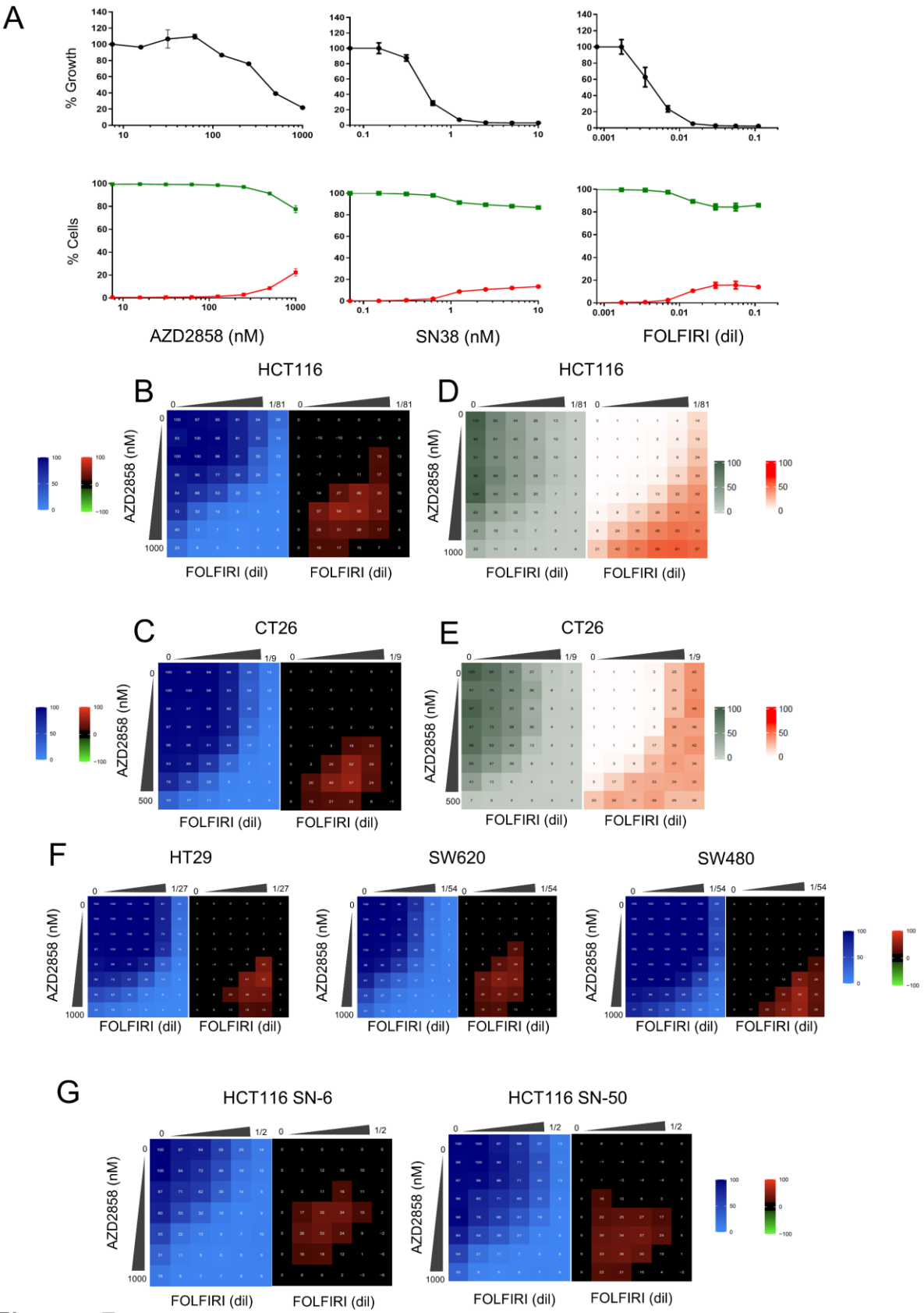
A
% Growth
% Cells
AZD2858 (nM)
SN38 (nM)
FOLFIRI (dil)
B
HCT116
D
HCT116
C
CT26
E
CT26
F
HT29
SW620
SW480
G
HCT116 SN-6
HCT116 SN-50
AZD2858 (nM)
FOLFIRI (dil)

Figure 5

Figure 5. The synergistic effect of the AZD2858 + FOLFIRI combination is due to cytotoxicity.
(**A**) HCT116 cells were incubated with increasing concentrations of each drug for 72 h. Then, dual staining with Hoechst/IP was performed to visualize dead cells (red) and live cells (green), respectively, in each well. Results were quantified using the dedicated Celigo® software and shown as percentages of dead cells and live cells relative to untreated controls. (**B**) HCT116 cells were incubated with increasing concentrations of FOLFIRI (5-FU from 0.009 to 0.148 µM and SN-38 from 0.077 to 1.235 nM) and AZD2858 (from 15.6 to 1000 nM). Cell viability was assessed with the SRB assay in 2D cultures to generate the viability matrix (blue). The synergy matrices (black and red) were calculated as described in Materials and Methods. (**C**) CT-26 cells were incubated with increasing concentrations of FOLFIRI (5-FU from 0.083 to 1.333 µM and SN-38 from 0.694 to 11.11 nM) and AZD2858 (from 7.8 to 500 nM). Cell viability was assessed with the SRB assay in 2D cultures to generate the viability matrix (blue). The synergy matrices were calculated as described in Materials and Methods. (**D**) HCT116 cells were incubated with increasing concentrations of FOLFIRI (5-FU from 0.009 to 0.148 µM and SN-38 from 0.077 to 1.235 nM) and AZD2858 (from 15.6 to 1000 nM) for 96 h. Then, dual staining with PI and Hoechst was performed to visualize dead cells (red) and live cells (green), respectively, in each well. Results were quantified using the dedicated Celigo® software: the green matrix represents cell survival and the orange matrix cell death, relative to untreated controls. (**E**) CT-26 cells were incubated with increasing concentrations of FOLFIRI (5-FU from 0.083 to 1.333 µM and SN-38 from 0.694 to 11.11 nM) and AZD2858 (from 7.8 to 500 nM) for 96 h. Then, dual staining with PI and Hoechst was performed to visualize dead cells (red) and live cells (green), respectively, in each well. Results were quantified using the dedicated Celigo® software; the green matrix represents cell survival and the orange matric cell death relative to untreated controls. (**F**) HT29, SW620 and SW480 CRC cells were incubated with increasing concentrations of FOLFIRI (HT29 cells: 5-FU from 0.03 to 1 µM and SN-38 from 0.07 to 2.35 nM; SW620 and SW480 cells: 5-FU: from 0.13 to 4.4 µM, SN-38: from 0.007 to 0.25 nM) and AZD2858 (from 15.6 to 1000 nM). Cell viability was assessed with the SRB assay in 2D cultures to obtain the viability matrix (blue). The synergy matrices (black and red) were calculated as described in Materials and Methods. (**G**) SN-38-resistant HCT116 SN-6 and HCT116 SN-50 cells were incubated with increasing concentrations of FOLFIRI (5-FU from 0.46 to 14.85 µM and SN-38 from 0.1 to 3.375 nM) and AZD2858 (from 15.6 to 1000 nM). Cell viability was assessed with the SRB assay in 2D cultures to generate the viability matrix (blue). The synergy matrices (black and red) were calculated as described in Materials and Methods.

Lastly, we tested the FOLFIRI+AZD2858 combination (matrix analysis) in 3D cell cultures that are physiologically closer to tumor growth compared with 2D cultures and allow mimicking the complexity of solid tumors from a structural, biochemical and biophysical point of view. We prepared spheroids of parental HCT116 cells, SN-38-resistant HCT116 SN-6 and HCT116 SN-50 cells, and murine CT-26 cells (**Figure 6 A-D**). We again observed that the combination was synergistic in all tested cell lines, demonstrating remarkable efficacy with nearly complete elimination of spheroids.

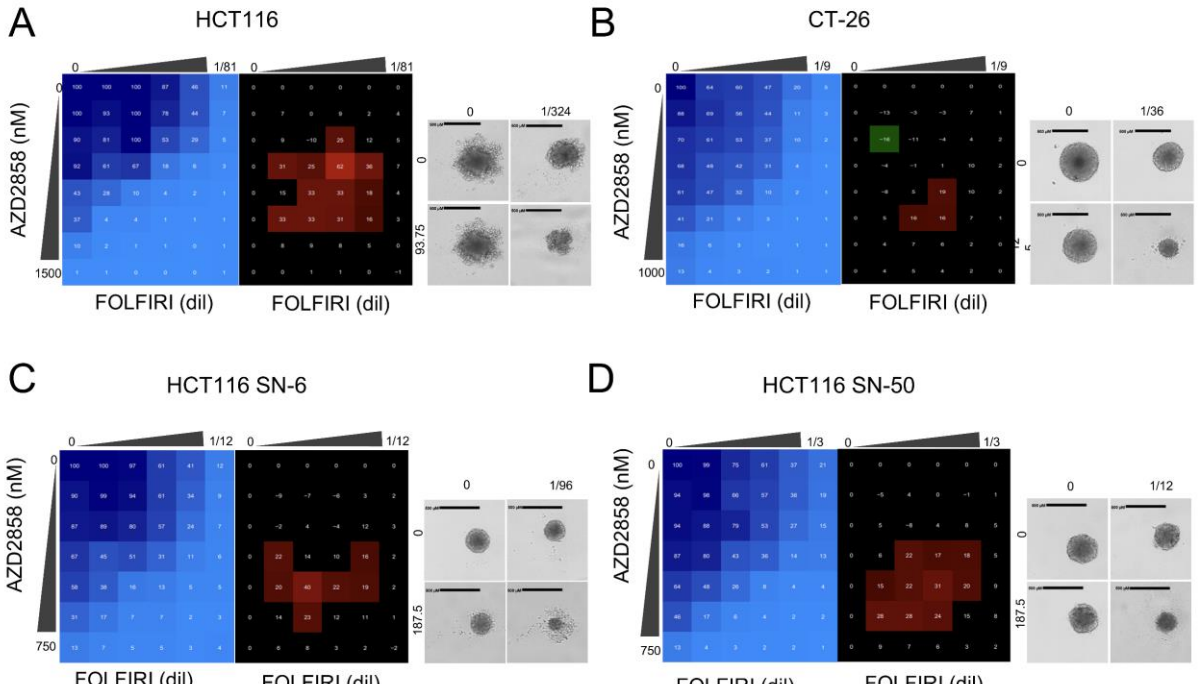

Figure 6

Figure 6. The AZD2858+FOLFIRI combination is synergistic in spheroids from human and murine CRC cell lines and also in spheroids of SN-38-resistant HCT116 cells.

(**A**) HCT116 cells were cultured in 3D and incubated with increasing concentrations of FOLFIRI (5-FU from 0.009 to 0.148 µM and SN-38 from 0.077 to 1.235 nM) and AZD2858 (from 23.4 to 1500 nM). Cell viability was assessed with CellTiter-Glo to obtain the viability matrix (blue). The synergy matrices (black and red) were calculated as described in Materials and Methods. Representative brightfield images of spheroids are shown: untreated and after incubation with the drug concentrations giving the highest synergy score. Experiments were replicated 3 times, and representative replicates are shown. (**B**) Same as in A but with the CT-26 murine cell line. Drug concentrations were as follows: FOLFIRI (5-FU from 0.083 to 1.333 µM and SN-38 from 0.694 to 11.1 nM) and AZD2858 (from 15.6 to 1000 nM). (**C**) Same as in A but with SN-38-resistant HCT116 SN-6 cells. Drug concentrations were as follows: FOLFIRI (5-FU from 0.083 to 1.333 µM and SN-38 from 0.694 to 11.1 nM) and AZD2858 (from 46.8 to 750 nM). (**D**) Same as in A but with SN-38-resistant HCT116 SN-50 cells. Drug concentrations were as follows: FOLFIRI (5-FU from 0.75 to 12 µM and SN-38 from 6.25 to 100 nM) and AZD2858 (from 46.8 to 750 nM).

Discussion

TopBP1 assembly is required for the activation of the ATR signaling pathway, a critical step in the DNA damage response and repair. We exploited our ability to control TopBP1 condensation and ATR activation using an optogenetic approach to develop a high-throughput screening procedure for identifying modulators of TopBP1 condensation. As proof of concept, we screened a TargetMol library of 4730 preclinical and clinical compounds. Through this approach, we found that AZD2858, a known GSK3-β inhibitor, is also a potential inhibitor of TopBP1 condensation. Using a complementary approach based on the irinotecan active metabolite SN-38 to induce DNA damage in CRC cells, we confirmed that AZD2858 disrupts endogenous TopBP1 condensates, thus affecting the ATR signaling pathway.

AZD2858 inhibits GSK-3β activity and activates the canonical Wnt/β-catenin signaling cascade (57). In addition, AZD2858 has cytotoxic effects in glioma cell lines through disruption of centrosome function and mitotic failure (58), and affects glioma proliferation and survival (57). Our findings show that AZD2858, at nanomolar concentrations, alters TopBP1 condensation without influencing GSK-3β activity and does not require the presence of GSK-3β to prevent Chk1 activation by SN-38. These observations clearly rule out the involvement of the GSK-3β pathway in TopBP1 condensate formation inhibition by AZD2858.

TopBP1 is overexpressed in several cancer types, including breast cancer (59) and advanced-stage CRC as well as radiotherapy-resistant lung cancer cells and oxaliplatin-resistant gastric cancer (43). This overexpression is associated with high-grade tumors and poor prognosis. Notably, inhibition of TopBP1 expression increases the radiosensitivity of lung cancer and brain metastases (60) and also DNA damage in oxaliplatin-resistant gastric cancer cells (43). To date, no study assessed or visualized TopBP1 condensate levels in tumors, or investigated whether their presence is linked to poor prognosis. Here, we found that TopBP1 condensates are increased in SN-38 resistant CRC cells. Many attempts have been made to target TopBP1 activity. Weei-Chin Lin's team was the first to perform two large scale molecular docking screens targeting the BRCT7/8 domains of TopBP1. They identified calcein AM and 5D4 as compounds that block TopBP1 oligomerization and demonstrated their anti-cancer activity *in vivo* (61,62). Interestingly, 5D4 also disrupts TopBP1 interaction with E2F1, mutant p53, CIP2A, and MIZ1, leading to E2F1-mediated apoptosis, suppression of mutant p53 and repression of MYC activity (61).

We demonstrated that AZD2858 disrupts the interaction between TopBP1 and its canonical partner ATR and also its self-interaction. Additionally, in cell-free *X. laevis* egg extracts, AZD2858, alone or in combination with the topoisomerase I inhibitor CPT, enhanced the DNA binding occupancy of both TopBP1 and RPA32. These findings, combined with the cell cycle and DNA fiber results, suggest that

AZD2858 abrogates the intra-S phase and DNA elongation checkpoints induced by SN-38, leading to unscheduled DNA synthesis. In addition, incubation with SN-38+AZD2858 enhanced DNA damage and apoptosis, as indicated by (i) the increased γH2AX levels, (ii) the persistence of DSBs (PFGE assay), (iii) the expression of cleaved PARP1 and caspase-3 (apoptotic markers), and (iv) the accumulation of sub-G1 cells. Incubation with the AZD2858+SN-38 combination mimicked the effects observed with ATR inhibitors when combined with topoisomerase I inhibitors, such as CPT, topotecan and SN-38 (55,62). For instance, the ATR inhibitors VE-821 and VE-822, sensitize cancer cells to CPT derivatives by alleviating the intra-S-phase checkpoint (55,62), and induce apoptosis mediated by caspase-3 when combined with SN-38 because cells experience extensive DNA damage due to failure of the replication checkpoint (55). Importantly, the efficacy of several ATR inhibitors is currently investigated in preclinical studies or in phase I/II clinical trials as monotherapy or in combination with chemotherapy-induced replication stress (63). We also showed a synergistic effect of the AZD2858+FOLFIRI combination, including in SN-38-resistant HCT116 cell lines, due to the increased apoptosis and accumulation of DNA damage. Given the similarity of mechanism between AZD2858 and ATR inhibitors, when combined with chemotherapy (SN-38 or CPT), we hypothesize that AZD2858 could prevent the development of resistance because its mechanism of action is not to inhibit the ATR kinase but to prevent the interaction of TopBP1 with ATR. FOLFIRI is used as first-line chemotherapy regimen for patients with metastatic CRC and gastric/gastroesophageal cancer (64).

In the last decade, a major advance has been made in our understanding of the mechanisms and functions of various cytoplasmic and nuclear membrane-less organelles within cells, revolutionizing the field of cell biology. Recent studies highlighted the importance of compartmentalizing cellular components into mesoscale structures, known as biomolecular condensates, implicated in new physiological functions and in triggering the activation of specific signaling pathways. Many research projects have incorporated condensates into the understanding of cancer pathogenesis, leading to the development of new therapeutic strategies to target cancer-associated condensates (65,66). We recently found that TopBP1 condensation acts as a molecular switch to amplify ATR activity (26), a critical pathway to tolerate the intrinsically high levels of lesions that block replication fork progression in cancer cells. Targeting TopBP1 assembly, rather than its degradation, offers an interesting strategy to selectively inhibit its role in the ATR/Chk1 signaling pathway activation, while preserving its other essential functions in replication and transcription that do not rely on its assembly.

Overall, this study brought the first insights into the rational of targeting the condensation of TopBP1, a multifunctional protein that forms biomolecular condensates in response to DNA damage to inhibit the ATR/Chk1 signaling pathway and to potentiate conventional therapies.

Acknowledgement

In memory of Angelos Constantinou whose significant contribution to the field of DNA damage response will remain an enduring source of inspiration for our research. We acknowledge the national infrastructure France-BioImaging supported by the French National Research Agency (ANR-10-INBS-04). This work was supported by the French Institut National du Cancer INCa (PLBIO 2021), by the French Agence Nationale de la Recherche ANR (AAPG2021), and by the Fondation MSD AVENIR. We acknowledge the MRI imaging core facility IRCM, a member of the National Infrastructure France-BioImaging for flow cytometry and CELIGO experiments and MRI CRBM for drug screening.

Author Contributions

Conceptualization: L.M, C.G, J.B, A.C; Methodology: L.M, N.V, A.A, T.E, A.Az, L.A.M, V.G, C.G, J.B; Formal analyses: L.M, N.V, A.A, T.E, A.Az, S.F, H.S, L.A.M, V.G; Investigation: L.M, A.A, N.V, C.G, J.B, A.C; Writing original draft: L.M, A.A, C.G, J.B, A.C; Writing – review and editing: L.M, A.A, T.E, C.G, J.B, A.C; Supervision: N.V, C.G, J.B, A.C; Project Administration: C.G, J.B, A.C; Funding acquisition N.V, C. G, A.C.

Declaration of Interests

The authors declare no competing interests.

Inclusion and diversity

We support inclusive, diverse, and equitable conduct of research.

References

1. Lindahl T, Barnes DE. Repair of endogenous DNA damage. Cold Spring Harb Symp Quant Biol. 2000;65:127-33.

2. Ciccia A, Elledge SJ. The DNA Damage Response: Making It Safe to Play with Knives. Mol Cell. oct 2010;40(2):179-204.

3. Jackson SP, Bartek J. The DNA-damage response in human biology and disease. Nature. 22 oct 2009;461(7267):1071-8.

4. Jackson SP, Helleday T. Drugging DNA repair. Science. 3 juin 2016;352(6290):1178-9.

5. Luo J, Solimini NL, Elledge SJ. Principles of cancer therapy: oncogene and non-oncogene addiction. Cell. 6 mars 2009;136(5):823-37.

6. Macheret M, Halazonetis TD. DNA replication stress as a hallmark of cancer. Annu Rev Pathol. 2015;10:425-48.

7. Brown JS, O'Carrigan B, Jackson SP, Yap TA. Targeting DNA Repair in Cancer: Beyond PARP Inhibitors. Cancer Discov. 1 janv 2017;7(1):20-37.

8. Brown EJ, Baltimore D. ATR disruption leads to chromosomal fragmentation and early embryonic lethality. Genes Dev. 15 févr 2000;14(4):397-402.

9. Eykelenboom JK, Harte EC, Canavan L, Pastor-Peidro A, Calvo-Asensio I, Llorens-Agost M, et al. ATR activates the S-M checkpoint during unperturbed growth to ensure sufficient replication prior to mitotic onset. Cell Rep. 27 nov 2013;5(4):1095-107.

10. de Klein A, Muijtjens M, van Os R, Verhoeven Y, Smit B, Carr AM, et al. Targeted disruption of the cell-cycle checkpoint gene ATR leads to early embryonic lethality in mice. Curr Biol. 20 avr 2000;10(8):479-82.

11. Tercero JA, Diffley JF. Regulation of DNA replication fork progression through damaged DNA by the Mec1/Rad53 checkpoint. Nature. 2 août 2001;412(6846):553-7.

12. Toledo LI, Altmeyer M, Rask MB, Lukas C, Larsen DH, Povlsen LK, et al. ATR prohibits replication catastrophe by preventing global exhaustion of RPA. Cell. 21 nov 2013;155(5):1088-103.

13. D'Angiolella V, Donato V, Forrester FM, Jeong YT, Pellacani C, Kudo Y, et al. Cyclin F-mediated degradation of ribonucleotide reductase M2 controls genome integrity and DNA repair. Cell. 25 mai 2012;149(5):1023-34.

14. Le TM, Poddar S, Capri JR, Abt ER, Kim W, Wei L, et al. ATR inhibition facilitates targeting of leukemia dependence on convergent nucleotide biosynthetic pathways. Nat Commun. 14 août 2017;8(1):241.

15. Lopez-Contreras AJ, Specks J, Barlow JH, Ambrogio C, Desler C, Vikingsson S, et al. Increased Rrm2 gene dosage reduces fragile site breakage and prolongs survival of ATR mutant mice. Genes Dev. 1 avr 2015;29(7):690-5.

16. Zhang YW, Jones TL, Martin SE, Caplen NJ, Pommier Y. Implication of checkpoint kinase-dependent up-regulation of ribonucleotide reductase R2 in DNA damage response. J Biol Chem. 3 juill 2009;284(27):18085-95.

17. Lecona E, Fernandez-Capetillo O. Targeting ATR in cancer. Nat Rev Cancer. sept 2018;18(9):586-95.

18. Ruiz S, Mayor-Ruiz C, Lafarga V, Murga M, Vega-Sendino M, Ortega S, et al. A Genome-wide CRISPR Screen Identifies CDC25A as a Determinant of Sensitivity to ATR Inhibitors. Mol Cell. 21 avr 2016;62(2):307-13.

19. Bhullar KS, Lagaron NO, McGowan EM, Parmar I, Jha A, Hubbard BP, et al. Kinase-targeted cancer therapies: progress, challenges and future directions. Mol Cancer. 19 févr 2018;17(1):48.

20. Mitrea DM, Mittasch M, Gomes BF, Klein IA, Murcko MA. Modulating biomolecular condensates: a novel approach to drug discovery. Nat Rev Drug Discov. nov 2022;21(11):841-62.

21. Banani SF, Lee HO, Hyman AA, Rosen MK. Biomolecular condensates: organizers of cellular biochemistry. Nat Rev Mol Cell Biol. mai 2017;18(5):285-98.

22. Mittag T, Pappu RV. A conceptual framework for understanding phase separation and addressing open questions and challenges. Mol Cell. 16 juin 2022;82(12):2201-14.

23. Kumagai A, Lee J, Yoo HY, Dunphy WG. TopBP1 Activates the ATR-ATRIP Complex. Cell. mars 2006;124(5):943-55.

24. Wardlaw CP, Carr AM, Oliver AW. TopBP1: A BRCT-scaffold protein functioning in multiple cellular pathways. DNA Repair Amst. oct 2014;22:165-74.

25. Zhou ZW, Liu C, Li TL, Bruhn C, Krueger A, Min W, et al. An essential function for the ATR-activation-domain (AAD) of TopBP1 in mouse development and cellular senescence. PLoS Genet. 2013;9(8):e1003702.

26. Frattini C, Promonet A, Alghoul E, Vidal-Eychenie S, Lamarque M, Blanchard MP, et al. TopBP1 assembles nuclear condensates to switch on ATR signaling. Mol Cell. janv 2021;S1097276520309916.

27. Koundrioukoff S, Carignon S, Técher H, Letessier A, Brison O, Debatisse M. Stepwise activation of the ATR signaling pathway upon increasing replication stress impacts fragile site integrity. PLoS Genet. 2013;9(7):e1003643.

28. Egger T, Morano L, Blanchard MP, Basbous J, Constantinou A. Spatial organization and functions of Chk1 activation by TopBP1 biomolecular condensates. Cell Rep [Internet]. 23 avr 2024 [cité 21 mai 2024];43(4). Disponible sur: https://www.cell.com/cell-reports/abstract/S2211-1247(24)00392-9

29. Duursma AM, Driscoll R, Elias JE, Cimprich KA. A Role for the MRN Complex in ATR Activation via TOPBP1 Recruitment. Mol Cell. avr 2013;50(1):116-22.

30. Acevedo J, Yan S, Michael WM. Direct Binding to Replication Protein A (RPA)-coated Single-stranded DNA Allows Recruitment of the ATR Activator TopBP1 to Sites of DNA Damage. J Biol Chem. 17 juin 2016;291(25):13124-31.

31. Mordes DA, Glick GG, Zhao R, Cortez D. TopBP1 activates ATR through ATRIP and a PIKK regulatory domain. Genes Dev. 1 juin 2008;22(11):1478-89.

32. Delacroix S, Wagner JM, Kobayashi M, Yamamoto K, Karnitz LM. The Rad9-Hus1-Rad1 (9-1-1) clamp activates checkpoint signaling via TopBP1. Genes Dev. 15 juin 2007;21(12):1472-7.

33. Lee J, Kumagai A, Dunphy WG. The Rad9-Hus1-Rad1 checkpoint clamp regulates interaction of TopBP1 with ATR. J Biol Chem. 21 sept 2007;282(38):28036-44.

34. Candeil L, Gourdier I, Peyron D, Vezzio N, Copois V, Bibeau F, et al. ABCG2 overexpression in colon cancer cells resistant to SN38 and in irinotecan-treated metastases. Int J Cancer. 10 mai 2004;109(6):848-54.

35. Cherradi S, Garambois V, Marines J, Andrade AF, Fauvre A, Morand O, et al. Improving the response to oxaliplatin by targeting chemotherapy-induced CLDN1 in resistant metastatic colorectal cancer cells. Cell Biosci. 11 avr 2023;13(1):72.

36. Skehan P, Storeng R, Scudiero D, Monks A, McMahon J, Vistica D, et al. New colorimetric cytotoxicity assay for anticancer-drug screening. J Natl Cancer Inst. 4 juill 1990;82(13):1107-12.

37. Tosi D, Pérez-Gracia E, Atis S, Vié N, Combès E, Gabanou M, et al. Rational development of synergistic combinations of chemotherapy and molecular targeted agents for colorectal cancer treatment. BMC Cancer. 13 août 2018;18:812.

38. Vezzio-Vié N, Kong-Hap MA, Combès E, Andrade AF, Del Rio M, Pasero P, et al. Multiplexed-Based Assessment of DNA Damage Response to Chemotherapies Using Cell Imaging Cytometry. Int J Mol Sci. 20 mai 2022;23(10):5701.

39. Li L, Kolinjivadi AM, Ong KH, Young DM, Marini GPL, Chan SH, et al. Automatic DNA replication tract measurement to assess replication and repair dynamics at the single-molecule level. Bioinformatics. 15 sept 2022;38(18):4395-402.

40. Goedhart J. SuperPlotsOfData—a web app for the transparent display and quantitative comparison of continuous data from different conditions. Mol Biol Cell. 15 mars 2021;32(6):470-4.

41. Whelan DR, Rothenberg E. Super-resolution mapping of cellular double-strand break resection complexes during homologous recombination. Proc Natl Acad Sci U S A. 16 mars 2021;118(11):e2021963118.

42. Wu ZX, Yang Y, Zeng L, Patel H, Bo L, Lin L, et al. Establishment and Characterization of an Irinotecan-Resistant Human Colon Cancer Cell Line. Front Oncol. 2020;10:624954.

43. Fang Z, Gong C, Ye Z, Wang W, Zhu M, Hu Y, et al. TOPBP1 regulates resistance of gastric cancer to oxaliplatin by promoting transcription of PARP1. DNA Repair. mars 2022;111:103278.

44. Association between the c.*229C>T polymorphism of the topoisomerase IIβ binding protein 1 (TopBP1) gene and breast cancer | Molecular Biology Reports [Internet]. [cité 7 mars 2024]. Disponible sur: https://link.springer.com/article/10.1007/s11033-012-2424-z

45. Candeil L, Gourdier I, Peyron D, Vezzio N, Copois V, Bibeau F, et al. ABCG2 overexpression in colon cancer cells resistant to SN38 and in irinotecan-treated metastases. Int J Cancer. 10 mai 2004;109(6):848-54.

46. Vezzio-Vié N, Kong-Hap MA, Combès E, Andrade AF, Del Rio M, Pasero P, et al. Multiplexed-Based Assessment of DNA Damage Response to Chemotherapies Using Cell Imaging Cytometry. Int J Mol Sci. 20 mai 2022;23(10):5701.

47. Kilic S, Lezaja A, Gatti M, Bianco E, Michelena J, Imhof R, et al. Phase separation of 53BP1 determines liquid-like behavior of DNA repair compartments. EMBO J. 15 août 2019;38(16):e101379.

48. Cescutti R, Negrini S, Kohzaki M, Halazonetis TD. TopBP1 functions with 53BP1 in the G1 DNA damage checkpoint. EMBO J. 3 nov 2010;29(21):3723-32.

49. Bigot N, Day M, Baldock RA, Watts FZ, Oliver AW, Pearl LH. Phosphorylation-mediated interactions with TOPBP1 couple 53BP1 and 9-1-1 to control the G1 DNA damage checkpoint. eLife. 28 mai 2019;8:e44353.

50. Cross DA, Alessi DR, Cohen P, Andjelkovich M, Hemmings BA. Inhibition of glycogen synthase kinase-3 by insulin mediated by protein kinase B. Nature. 21 déc 1995;378(6559):785-9.

51. Alghoul E, Basbous J, Constantinou A. An optogenetic proximity labeling approach to probe the composition of inducible biomolecular condensates in cultured cells. STAR Protoc. 17 sept 2021;2(3):100677.

52. Branon TC, Bosch JA, Sanchez AD, Udeshi ND, Svinkina T, Carr SA, et al. Efficient proximity labeling in living cells and organisms with TurboID HHS Public Access Author manuscript. Nat Biotechnol. 2018;36(9):880-7.

53. Marheineke K, Hyrien O. Control of Replication Origin Density and Firing Time in Xenopus Egg Extracts. J Biol Chem. juill 2004;279(27):28071-81.

54. Stracker TH, Usui T, Petrini JHJ. Taking the time to make important decisions: the checkpoint effector kinases Chk1 and Chk2 and the DNA damage response. DNA Repair. 2 sept 2009;8(9):1047-54.

55. Egger T, Bordignon B, Coquelle A. A clinically relevant heterozygous ATR mutation sensitizes colorectal cancer cells to replication stress. Sci Rep. 31 mars 2022;12(1):5422.

56. Gongora C, Vezzio-Vie N, Tuduri S, Denis V, Causse A, Auzanneau C, et al. New Topoisomerase I mutations are associated with resistance to camptothecin. Mol Cancer. 27 mai 2011;10:64.

57. Gao L, Chen B, Li J, Yang F, Cen X, Liao Z, et al. Wnt/β-catenin signaling pathway inhibits the proliferation and apoptosis of U87 glioma cells via different mechanisms. PloS One. 2017;12(8):e0181346.

58. Brüning-Richardson A, Shaw GC, Tams D, Brend T, Sanganee H, Barry ST, et al. GSK-3 Inhibition Is Cytotoxic in Glioma Stem Cells through Centrosome Destabilization and Enhances the Effect of Radiotherapy in Orthotopic Models. Cancers. 25 nov 2021;13(23):5939.

59. Forma E, Krzeslak A, Bernaciak M, Romanowicz-Makowska H, Brys M. Expression of TopBP1 in hereditary breast cancer. Mol Biol Rep. 2012;39(7):7795-804.

60. Choi SH, Yang H, Lee SH, Ki JH, Nam DH, Yoo HY. TopBP1 and Claspin contribute to the radioresistance of lung cancer brain metastases. Mol Cancer. déc 2014;13(1):211.

61. Lin FT, Liu K, Garan LAW, Folly-Kossi H, Song Y, Lin SJ, et al. A small-molecule inhibitor of TopBP1 exerts anti-MYC activity and synergy with PARP inhibitors. Proc Natl Acad Sci. 31 oct 2023;120(44):e2307793120.

62. Chowdhury P, Lin GE, Liu K, Song Y, Lin FT, Lin WC. Targeting TopBP1 at a convergent point of multiple oncogenic pathways for cancer therapy. Nat Commun. 17 nov 2014;5(1):5476.

63. Qiu Z, Oleinick NL, Zhang J. ATR/CHK1 inhibitors and cancer therapy. Radiother Oncol. mars 2018;126(3):450-64.

64. Van Cutsem E, Nordlinger B, Cervantes A. Advanced colorectal cancer: ESMO Clinical Practice Guidelines for treatment. Ann Oncol. mai 2010;21:v93-7.

65. Suzuki HI, Onimaru K. Biomolecular condensates in cancer biology. Cancer Sci. févr 2022;113(2):382-91.

66. Boija A, Klein IA, Young RA. Biomolecular Condensates and Cancer. Cancer Cell. févr 2021;39(2):174-92.

Supplementary data

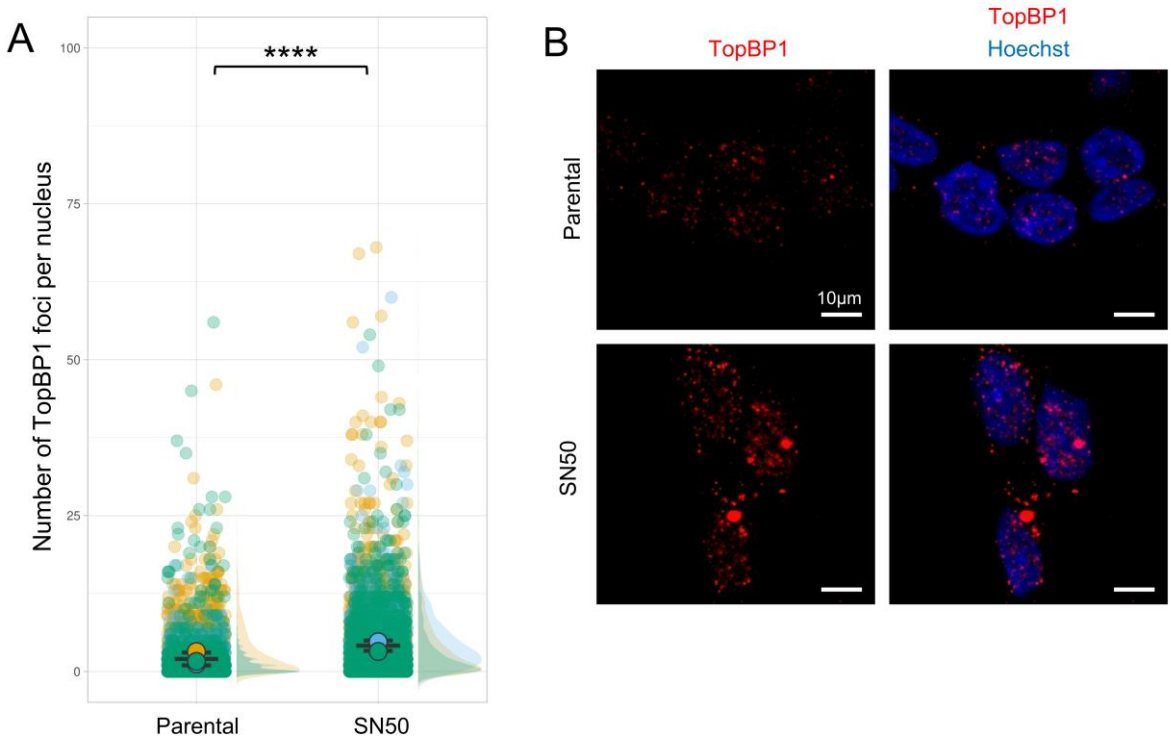

Figure S1. TopBP1 forms more foci in SN-38-resistant HCT116 cells.
(**A**) Number of TopBP1 foci per cell in parental and SN-38-resistant HCT116 cells. Data were pooled from n = 3 biological replicates (yellow, blue, green). Data distribution is shown as a half-violin plots on the right. Circles represent the mean of each replicate, and the error bars represent the SEM of the means of the three replicates. Significance of the differences was tested using an ANOVA on a generalized linear model interrogating both the effect of cell line genotype and replicate identity (modeling TopBP1 foci number by a Poisson distribution). Foci numbers are significantly different between the two cell lines (p-value<2.2e-16) and across the 3 replicates of the experiment (p-value<2.2e-16). (**B**) Representative images of one replicate.

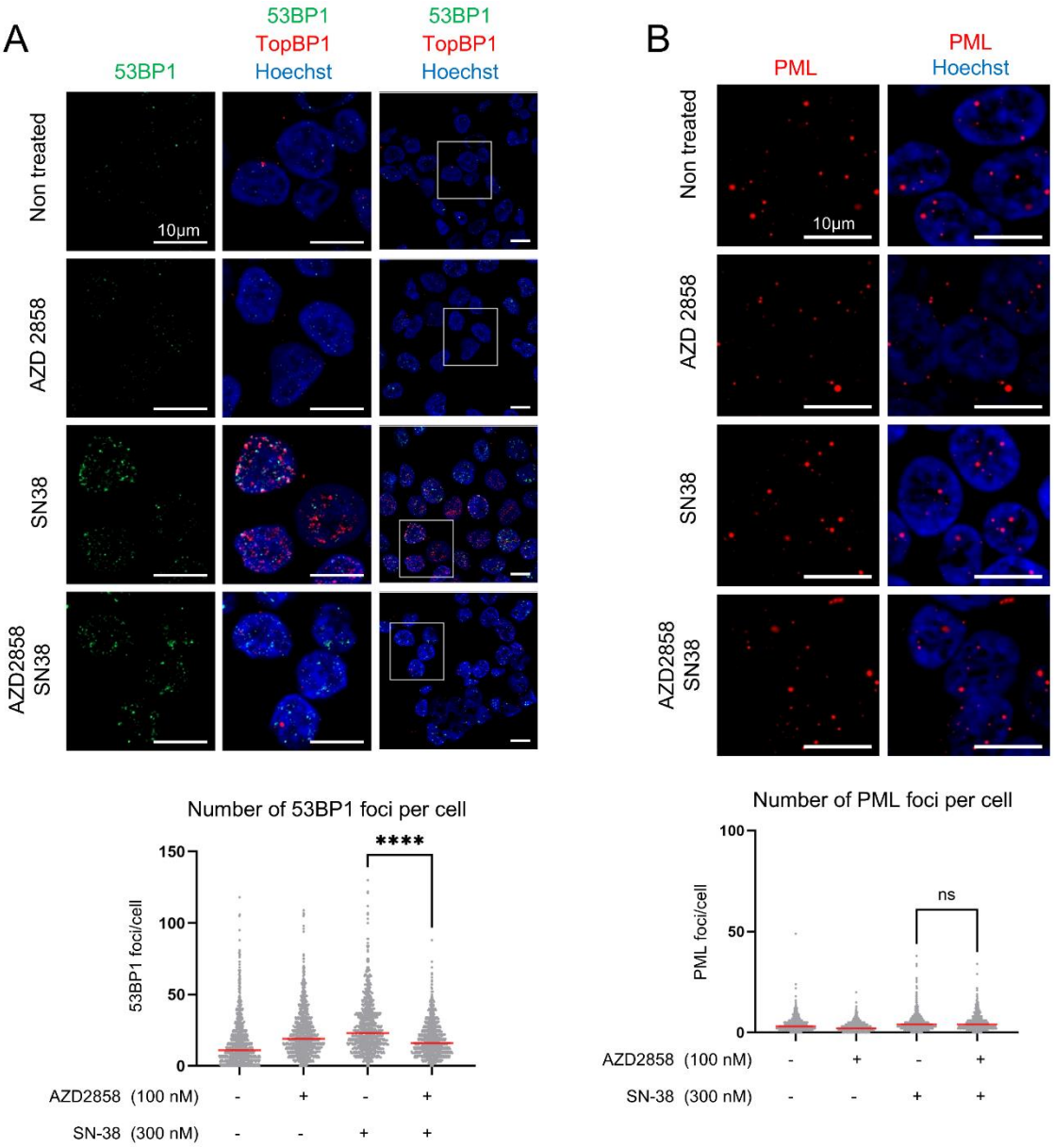

Figure S2. Impact of the AZD2858 + SN-38 combination on two nuclear biomolecular condensates.
(**A**) The effect of AZD2858 (100 nM) or/and SN-38 (300 nM) on 53BP1 and (**B**) PML condensates was tested after 2 h of incubation. Scale bars, 10µm; ns: non-significant; ****: p<0.0001 (Mann-Whitney test).

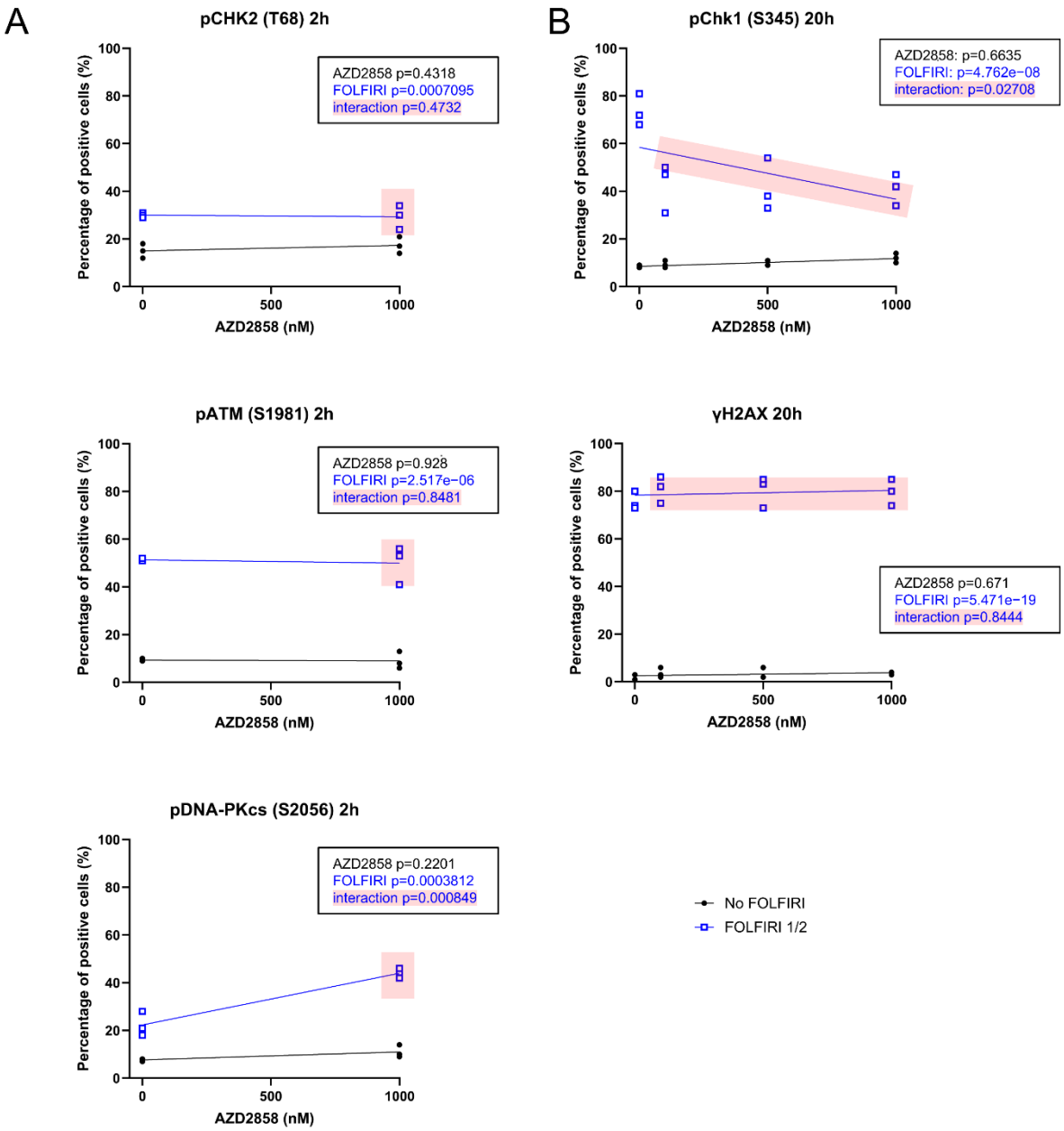

Figure S3. Effects of AZD2858 on components of the DNA damage response.

(**A**) Quantification of the percentage of phosphorylated Chk2 (pChk2) (T68), pATM (S1981) and pDNA-PKcs (S2056)-positive cells in HCT116 CRC cells incubated with FOLFIRI (5-FU: 6 µM and SN-38: 50 nM) and increasing concentrations of AZD2858 (from 250 to 1000 nM) for 2 h and (**B**) of pChk1 and γH2AX-positive cells after incubation for 20 h. Data were obtained by immunofluorescence analysis using the "Expression analysis" application of the Celigo Imaging Cytometer (Nexcelom). The combination of FOLFIRI and AZD2858 is shaded in pink. The experiment was replicated 3 times, and each point represents a biological replicate. The statistical significance was determined by linear modeling analysis interrogating the effect of each drug separately, and of their interaction (p-values given in the inset).

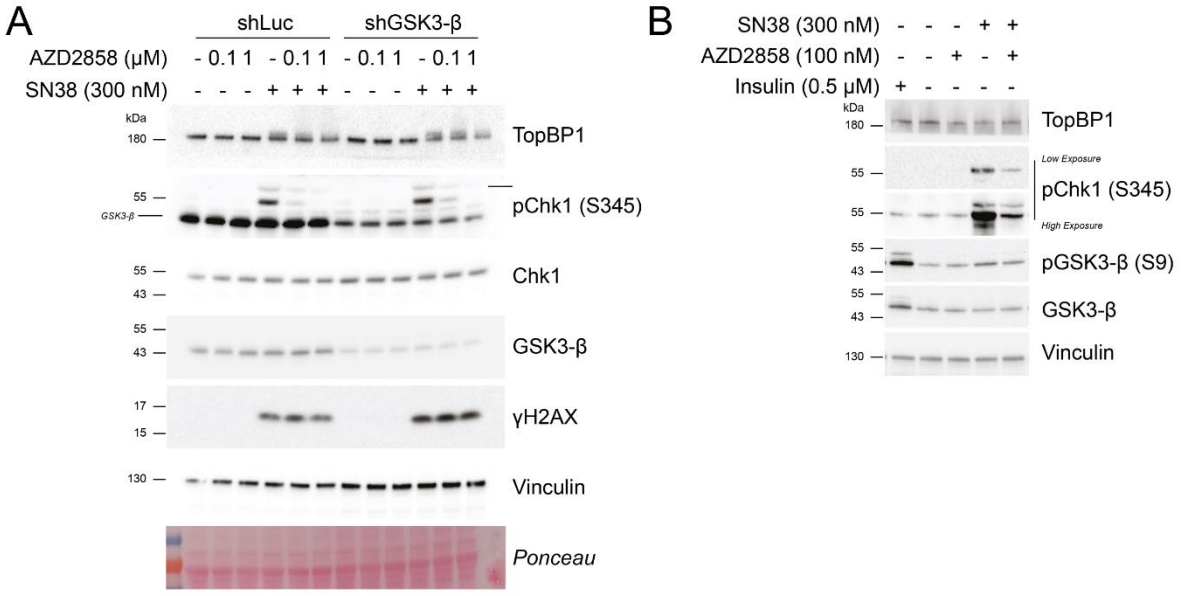

Figure S4. AZD2858 effect on ATR signaling is not related to GSK-3β activity.

(**A**) Immunoblot of the indicated proteins after incubation of SW620 cells that express shLuc or shGSK-3β with AZD2858 (100 nM) or/and SN-38 (300 nM) for 2 h. (**B**) Immunoblot of indicated proteins after incubation of HCT116 cells with AZD2858 (100 nM) or/and SN-38 (300 nM), or insulin (0.5 μM) (positive control of GSK-3β inhibition).

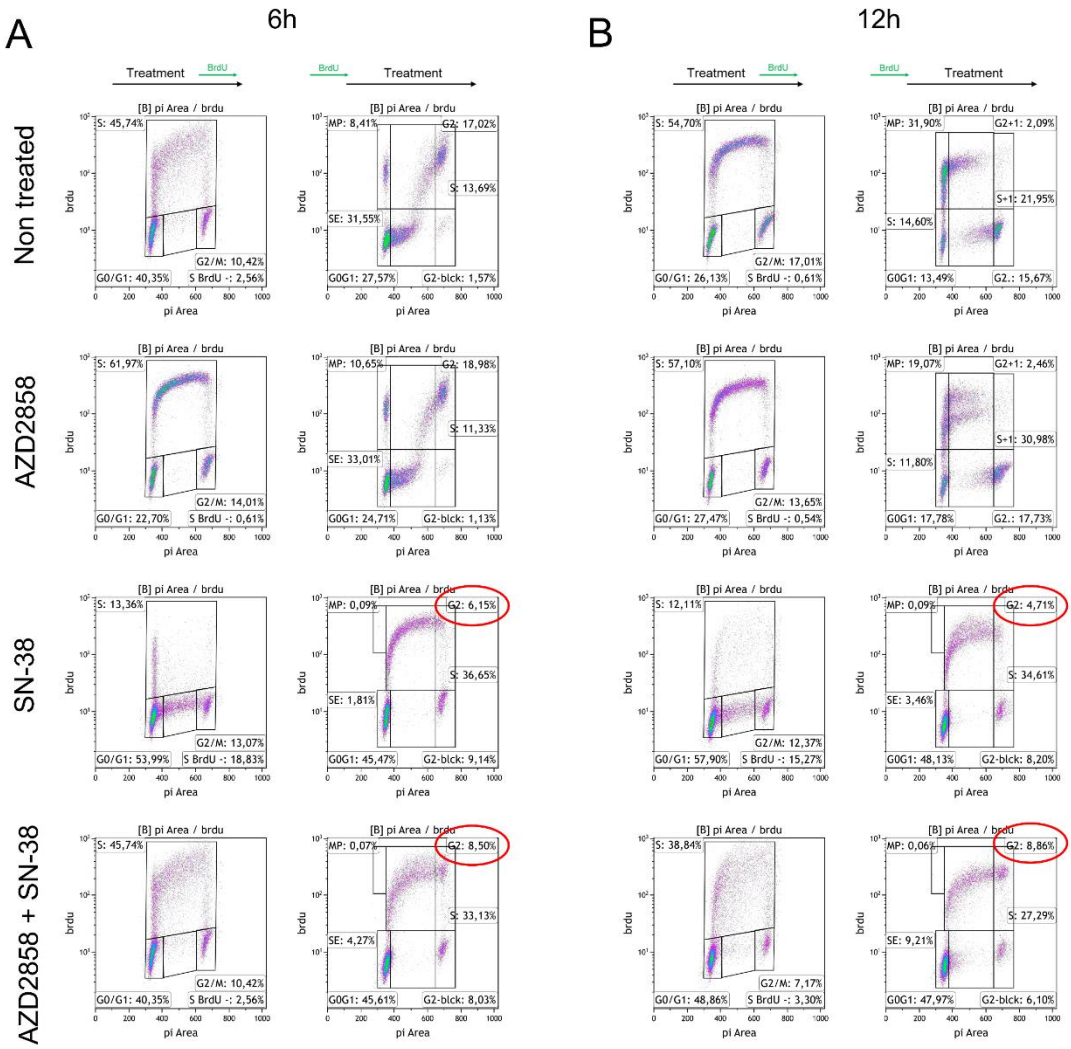

Figure S5. Cell-cycle profiling of HCT116 cells incubated with AZD2858 or/and SN-38.
(**A**) Cells were incubated with AZD2858 (100 nM) and/or SN-38 (300 nM) for 6 h. In the left panels, cells were incubated with BrdU for the last 15 min of the treatments (biological replicates of Figure 3C). In the right panels, cells were pulsed with BrdU for 15 min before the treatments, then chased without BrdU for the 6 hours of treatment. Cellular debris were gated out and the level of BrdU incorporation was plotted against the DNA content. 20,000 events per condition were analyzed. BrdU-positive cells include "MP" (mitotic passage, cells that were in S phase during the pulse, completed mitosis, and returned to a 2N DNA content), "S" (cells in S phase during the pulse and still in S phase at the endpoint), and "G2" (cells in S phase during the pulse that progressed to 4N DNA). Among the BrdU-negative cells, G0/G1 cells had a 2N DNA content after the chase. BrdU-negative cells with >2N DNA content entered S-phase after the BrdU pulse and were gated “SE” for S-phase entry. "G2-blocked" 4N cells were already in G2/M during the BrdU pulse and were still blocked at the endpoint. (**B**) Same as in A) but after 12 h of treatment. The gate of interest (G2 phase) and the corresponding cell percentages are outlined in red. The experiment was replicated 3 times, and a representative replicate is shown.

GSK-3 inhibitors in the library	Specificity	Specificity to GSK-3β (IC50)	Light-induced inhibition of TopBP1 foci	SN-38-induced Chk1 phosphorylation (pChk1) inhibition	Source for IC50 data
6-BIO	5 nM (α/β)	+++	no		Selleckchem
9-ING-41	N/A	N/A	no		Selleckchem
AR-A014418	38 nM (β)	++	no		Selleckchem
AT 7519 hydrochloride salt	89 nM (α/β?)	+ (?)	yes (-3.4)	N/A	Raybiotech
AT7519	N/A	N/A	no		Selleckchem
AZD1080	31 nM (β) 6.9 nM(α)	++	no		Selleckchem
AZD2858	5 nM (β) 0.9 nM (α)	+++	yes (-3.6)	yes	Medchemexpress
Bikinin	N/A	N/A	no		Selleckchem
BIO-acetoxime	10 nM (α/β)	++	yes (-3.7)	no	Selleckchem
BRD0705	515 nM (β)	+	No		Selleckchem
CHIR98014	0.58 nM(β) 0.65 nM (α)	++++	yes (-2.8)	N/A	Selleckchem
CHIR99021	6.7 nM (β) 10 nM (α)	+++	no		Selleckchem
CP21R7	N/A	N/A	no		Selleckchem
Ginsenoside Rg2	N/A	N/A	no		N/A
GSK3i XIII	24 nM (?) Ki	++	yes (-4.3)	N/A	Sigma
GSK-3β inhibitor 1	4.19 nM	+++	no		Selleckchem
IM12	53 nM (β)	+	no		Selleckchem
Indirubin	600 nM (β)	+	no		Selleckchem
Indirubin-3'-monoxime	190 nM	+	yes (-2.2)	N/A	Tocris
KenPaullone	230 nM (β)	+	no		Selleckchem
KY19382	10 nM(β)	++	no		Medchemexpress+selleckchem
Lithium citrate tribasic tetrahydrate	N/A	N/A	no		N/A
LY2090314	0.9 nM (β) 1.5 nM (α)	++++	yes (-3.4)	no	Selleckchem
PHA767491 HCl	N/A	N/A	no		Selleckchem
SB216763	34.3 nM (α/β)	++	no		Selleckchem
SB415286	78 nM (α/β)	+	no		Selleckchem
TBB	N/A	N/A	no		N/A
TDZD8	200 nM (β)	+	no		Selleckchem
Tideglusib	60 nM (β)	+	no		Selleckchem
TWS119	30 nM (β)	++	yes (-2.8)	N/A	Selleckchem
VP3.15 dihydrobromide	880 nM (α/β ?)	+ (?)	no		Medchemexpress

Table S1. GSK-3 inhibitors present in the TargetMol library.

The Specificity column indicates the IC_{50} values available in the literature corresponding to 50% of the maximal concentration needed to inhibit the GSK-3 target (except for GSK3i XIII, where only the inhibition constant, Ki, value was available). The GSK-3β specificity column indicates the specificity toward this isoform, if available. If specificity was determined, but the GSK-3β isoform was not clearly specified, a question mark is used to indicate this uncertainty (for VP3.15 dihydrobromide and AT 7519 hydrochloride salt). ++++: < 1 nM; +++: between 1 nM and 10 nM; ++: between 10 nM and 40 nM; +: > 40 nM. Molecules that inhibited light-induced optoTopBP1 foci in the present screen are highlighted in red, and the z-score is indicated. The SN-38-induced Chk1 phosphorylation (pChk1) inhibition column indicates whether the potential GSK-3 inhibitors from the initial screen inhibit SN-38-induced Chk1 phosphorylation at S345 in HCT116 cells. N/A: Not Available.

Estimation of effect (amplitude and *p*-value) by linear modeling:

Effect of experimental condition (compared with "NT") :

Condition	Effect on percentage of subG1	*p*-value
A	-0.05329	0.99220
AF	+56.43905	9.19e-07
AS	+46.09911	5.79e-06
F	+17.95105	0.00706
S	+9.60998	0.10089

Effect of experimental condition (compared with "S") :

Condition	Effect on percentage of subG1	*p*-value
NT	-9.610	0.10089
A	-9.663	0.09926
AF	+46.829	5.03e-06
AS	+36.489	4.40e-05
F	+8.341	0.14786

Effect of experimental condition (compared with "F") :

Condition	Effect on percentage of subG1	*p*-value
S	-8.341	0.147855
NT	-17.951	0.007057
A	-18.004	0.006939
AF	+38.488	2.8e-05
AS	+28.148	0.000351

Effect of replicate identity (compared with replicate #1) :

Replicate	Effect on percentage of subG1	*p*-value
2	+12.45762	0.00784
3	+11.50860	0.01204

Table S2. Results of the linear regression analysis (Figure 5A-B).

NT: Non-Treated. A: AZD2858. S: SN-38. F: FOLFIRI (5-FU + SN-38). The p-values of interest from Figure 5B are indicated in red.

FOLFIRI concentration range (dilution 1/1 = 12 µM 5-FU + 100 nM SN-38)						
HCT116 (2D & 3D)	**FOLFIRI (dilution factor)**	**1296**	**648**	**324**	**162**	**81**
	5-FU (µM)	0.009	0.019	0.037	0.074	0.148
	SN-38 (nM)	0.077	0.154	0.309	0.617	1.235
CT26 (2D & 3D)	**FOLFIRI (dilution factor)**	**144**	**72**	**36**	**18**	**9**
	5-FU (µM)	0.083	0.167	0.333	0.667	1.333
	SN-38 (nM)	0.694	1.389	2.778	5.556	11.111
HT29 (2D)	**FOLFIRI (dilution factor)**	**432**	**216**	**108**	**54**	**27**
	5-FU (µM)	0.028	0.056	0.111	0.222	0.444
	SN-38 (nM)	0.231	0.463	0.926	1.852	3.704
SW620 (2D)	**FOLFIRI (dilution factor)**	**864**	**432**	**216**	**108**	**54**
	5-FU (µM)	0.014	0.028	0.056	0.111	0.222
	SN-38 (nM)	0.116	0.231	0.463	0.926	1.852
SW480 (2D)	**FOLFIRI (dilution factor)**	**864**	**432**	**216**	**108**	**54**
	5-FU (µM)	0.014	0.028	0.056	0.111	0.222
	SN-38 (nM)	0.116	0.231	0.463	0.926	1.852
HCT116-SN6 (2D) HCT116-SN50 (2D)	**FOLFIRI (dilution factor)**	**32**	**16**	**8**	**4**	**2**
	5-FU (µM)	0.375	0.750	1.500	3.000	6.000
	SN-38 (nM)	3.125	6.250	12.500	25.000	50.000
HCT116-SN6 (3D)	**FOLFIRI (dilution factor)**	**192**	**96**	**48**	**24**	**12**
	5-FU (µM)	0.063	0.125	0.250	0.500	1.000
	SN-38 (nM)	0.521	1.042	2.083	4.167	8.333
HCT116-SN50 (3D)	**FOLFIRI (dilution factor)**	**48**	**24**	**12**	**6**	**3**
	5-FU (µM)	0.250	0.500	1.000	2.000	4.000
	SN-38 (nM)	2.083	4.167	8.333	16.667	33.333

Table S3. FOLFIRI concentration ranges used for the synergy matrix assays.
All the dilutions are based on the dilution 1/1 corresponding to 12 µM 5-fluorouracil (5-FU) and 100 nM SN-38.

Target	Compagny	Reference	Species	Dilution Celigo	Dilution WB	Dilution IF
H3	Cell Signaling Technology	#4499	Rabbit		1/1000	
α-Tubulin	Sigma	#T5168	Mouse		1/10000	
53BP1	Abcam	#ab175933	Rabbit			1/100
ATR	Bethyl	#A300-137A	Rabbit		1/1000	
Chk1	Santa Cruz Biotechnology	#sc-8408	Mouse		1/1000	
Chk2	Milipore	#05-649	Mouse		1/1000	
GSK-3β	Cell Signaling Technology	#9832	Mouse		1/1000	
GSK-3β (S9)	Cell Signaling Technology	#9336	Rabbit		1/1000	
H2B						
pATM (T1981)	Santa Cruz	#sc-47739	Mouse	1/100		
pATM (T1981)	Rockland	#200-301-40	Mouse		1/1000	
pATR (T1989)	Euromedex	#GTX128145	Rabbit	1/1000	1/1000	
pChk1 (S345)	Cell Signaling	#2348	Rabbit	1/50	1/1000	
pChk2 (T68)	Cell signaling	#2661	Rabbit	1/50	1/1000	
pDNA-PKcs (S2056)	Abcam	#ab124918	Rabbit	1/200		
pDNA-PKcs (S2056)	Abcam	#ab18192	Rabbit		1/1000	
PML	Santa Cruz	#sc-966	Mouse			1/100
Pol ε	Kind gift from Shou Waga	#N/A				
pRPA32 (S33)	Abcam	#ab2118877	Rabbit			
pRPA32 (S4/8)	Euromedex	#A300-245A	Rabbit		1/1000	
RPA32	Abcam	#ab2175	Mouse		1/1000	
RPA34						
TopBP1	Santa Cruz	#sc-271043	Mouse			1/100
TopBP1	Euromedex	#A300-111A	Rabbit		1/1000	
Vinculin	Merck	#V9131	Mouse		1/10000	
γH2AX (S139)	Cell signaling	#9718S	Rabbit		1/1000	
γH2AX (S139)	Abcam	#ab1195189	Rabbit	1/1000		

Table S4. References of the antibodies used in the study.
WB, western blotting; IF, immunofluorescence analyses.